Plant Physiology®

Plant Physiology, 2025, **197**, kiaf120
https://doi.org/10.1093/plphys/kiaf120
Advance access publication 27 March 2025
Research Article

Mutations in *HEADING DATE 1* affect transcription and cell wall composition in rice

Marco Biancucci,[1,†] Daniele Chirivì,[1,†] Alessio Baldini,[1] Eugene Badenhorst,[2] Fabio Dobetti,[1] Bahman Khahani,[3] Elide Formentin,[4] Tenai Eguen,[5] Franziska Turck,[6] John P. Moore,[2] Elahe Tavakol,[7] Stephan Wenkel,[5,8] Fiorella Lo Schiavo,[4] Ignacio Ezquer,[1] Vittoria Brambilla,[9] David Horner,[1] Matteo Chiara,[1] Giorgio Perrella,[1] Camilla Betti,[1] Fabio Fornara[1,*]

[1]Department of Biosciences, University of Milan, Via Celoria 26, Milan 20133, Italy
[2]South African Grape and Wine Research Institute, Department of Viticulture and Oenology, Stellenbosch University, Stellenbosch 7600, South Africa
[3]Plant Biology Graduate Program, University of Massachusetts, Amherst, MA 01003, USA
[4]Department of Biology, University of Padua, Viale Colombo 3, Padua 35131, Italy
[5]Copenhagen Plant Science Centre, University of Copenhagen, Thorvaldsensvej 40, Frederiksberg C 1871, Denmark
[6]Department of Plant Developmental Biology, Max Planck Institute for Plant Breeding Research, Carl-von-Linne-Weg 10, 50829 Köln, Germany
[7]Department of Plant Genetics and Production, College of Agriculture, Shiraz University, Shiraz, PHQM+92W, Iran
[8]Umeå Plant Science Centre, Umeå University, Umeå 90187, Sweden
[9]Department of Agricultural and Environmental Sciences—Production, Territory, Agroenergy, University of Milan, Via Celoria 2, Milan 20133, Italy
*Author for correspondence: fabio.fornara@unimi.it
[†]These authors contributed equally.
The author responsible for distribution of materials integral to the findings presented in this article in accordance with the policy described in the Instructions for Authors (https://academic.oup.com/plphys/pages/General-Instructions) is: Fabio Fornara (fabio.fornara@unimi.it).

Abstract

Plants utilize environmental information to modify their developmental trajectories for optimal survival and reproduction. Over a century ago, day length (photoperiod) was identified as a major factor influencing developmental transitions, particularly the shift from vegetative to reproductive growth. In rice (*Oryza sativa*), exposure to day lengths shorter than a critical threshold accelerates flowering, while longer days inhibit this process. This response is mediated by HEADING DATE 1 (Hd1), a zinc finger transcription factor that is central in the photoperiodic flowering network. Hd1 acts as a repressor of flowering under long days but functions as a promoter of flowering under short days. However, how global transcription of genes downstream of *Hd1* changes in response to the photoperiod is still not fully understood. Furthermore, it is unclear whether Hd1 target genes are solely involved in flowering time control or mediate additional functions. In this study, we utilized RNA-Seq to analyze the transcriptome of *hd1* mutants under both long and short day conditions. We identified genes involved in the phenylpropanoid pathway that are deregulated under long days in the mutant. Quantitative profiling of cell wall components and abiotic stress assays suggested that Hd1 is involved in processes considered unrelated to flowering control. This indicates that day length perception and responses are intertwined with physiological processes beyond flowering.

Introduction

The timing of flowering is an important adaptive trait for all plant species. It allows synchronization of the reproductive phase with optimal seasonal conditions and among individuals, thus maximizing seed set. This feature is particularly relevant for crop species because it sets cycle length, ensures maximal yields, and facilitates field management. The trait is under tight genetic and environmental control, and a very large number of flowering time genes, arranged in regulatory networks, work at the interface between monitoring endogenous and external parameters and promoting or repressing flower development.

Several factors can influence seasonal flowering, including aging and hormones, water and nutrient availability, biotic and abiotic stresses, fluctuating temperatures and light conditions (Song et al. 2015; Vicentini et al. 2023). However, among all parameters, changes in day length (photoperiod) are the most informative because their pattern is invariant from year to year and therefore predictable and reliable for anticipating seasonal changes. Plants have evolved the capacity to measure and respond to day length variations and can be categorized as long (LD) or short day (SD) species, depending on the condition that promotes flowering. Day neutral behaviors are also observed, wherein species do not use the photoperiod as an environmental cue to control flowering.

Rice (*Oryza sativa*) is a facultative SD plant, in which flowering is accelerated when the photoperiod falls below a critical threshold (Itoh et al. 2010). Its progenitors can be found in tropical and subtropical regions (Wang et al. 2018; Jing et al. 2023). However, breeding efforts have succeeded in expanding cultivation also to higher latitudes, characterized by LD during the cropping season, in both Asia and Europe (Gómez-Ariza et al. 2015; Goretti et al. 2017; Zong et al. 2021; Sun et al. 2022).

A complex regulatory network, principally constituted by photoreceptors and transcription factors, measures day length, and determines flowering time. The *HEADING DATE 1* (*Hd1*) gene was the first component of the rice photoperiodic network to be cloned

Received January 30, 2025. Accepted February 18, 2025.

and is a homolog of *CONSTANS* (*CO*), a photoperiod sensor of Arabidopsis (Yano et al. 2000). Both genes encode transcription factors characterized by the presence of B-Box zinc finger domains at the N-terminus and of a CONSTANS, CO-like, and TOC1 (CCT) domain at their C-terminus, which are required for protein-protein interactions and DNA binding. *Hd1* and *CO* are not orthologs, and their recruitment in the photoperiodic network is likely the result of convergent evolution (Ballerini and Kramer 2011; Simon et al. 2015; Vicentini et al. 2023). Functionally, *Hd1* promotes flowering under SD, by inducing transcription of *HEADING DATE 3a* (*Hd3a*) and *RICE FLOWERING LOCUS T 1* (*RFT1*), encoding rice florigens. Its activity reverts under LD, and *Hd1* becomes a repressor of flowering and of *Hd3a* and *RFT1* expression. *CO* shows a similar photoperiod-dependent functional reversion, promoting flowering under LD and repressing it under SD, although its SD repressive activity is not dependent upon reduction of florigen expression (Luccioni et al. 2019).

The Hd1 protein forms higher-order heterotrimeric NUCLEAR FACTOR Y (NF-Y) complexes, interacting with NF-YB and NF-YC subunits (Goretti et al. 2017; Shen et al. 2020). This feature is typical of proteins containing a CCT domain and occurs among both monocot and dicot species (Wenkel et al. 2006; Li et al. 2011; Goretti et al. 2017; Shen et al. 2020). NF-YB and NF-YC form histone-like dimers that have nonsequence specific affinity for DNA. When a CCT domain protein is incorporated, the trimer binds specifically to sequences containing a CO-Responsive Element (*CORE*). Initial studies on Arabidopsis defined the *CORE* as *TGTG(N2-3)ATG* (Wenkel et al. 2006; Adrian et al. 2010; Tiwari et al. 2010; Gnesutta et al. 2017). Subsequent work narrowed down the *CORE* to *TGTGGT* (for potato StCOL1) and *TGTGG* (for Arabidopsis CO and rice Hd1) (Abelenda et al. 2016; Gnesutta et al. 2017; Goretti et al. 2017). The crystal structures of CO and Hd1, in complex with NF-YB/C subunits and DNA, have further refined the *CORE*, indicating that essential contacts are made with a *TGTG* motif only (Shen et al. 2020; Chaves-Sanjuan et al. 2021; Lv et al. 2021).

Rice NF-Y can accommodate distinct DNA binding subunits containing a CCT domain. These include GRAIN YIELD PLANT HEIGHT AND HEADING DATE 7 (Ghd7), PSEUDO RESPONSE REGULATOR 37 (PRR37) and PRR73 (Shen et al. 2020; Liang et al. 2021). Changing the DNA binding subunit might modify preference of the trimer for motifs recognition. However, comparison of available binding motifs, identified by chromatin immunoprecipitation, SELEX, or other techniques, suggests that all CCT domain proteins might bind a *TGTG* core sequence (Gnesutta et al. 2018).

The rice NF-YB and NF-YC subunits belong to expanded families, comprising 11 and 7 genes, respectively, indicating a certain degree of redundancy and/or cooperativity (Petroni et al. 2012). The *OsNF-YB11* gene encodes for Ghd8/DAYS TO HEADING 8 (DTH8)/HEADING DATE 5 (Hd5) (hereafter Ghd8), a major LD repressor in the photoperiod pathway (Wei et al. 2010). The OsNF-YB7, 8, 9 and 10 proteins have similar activities, although not as central as Ghd8, and could replace Ghd8 in the heterotrimer (Hwang et al. 2016; Li et al. 2016). Similarly, biochemical and genetic evidence point to redundant roles for OsNF-YC1, 2, 4 and 7 (Kim et al. 2016; Goretti et al. 2017; Shen et al. 2020). A direct interaction between Hd1 and Ghd7 has also been reported, suggesting that NF-Y complexes might include more than 1 CCT protein, or that multiple NF-Y complexes interact through their CCT components (Nemoto et al. 2016; Gnesutta et al. 2018). Hd1 and Ghd7 repress expression of *EARLY HEADING DATE 1* (*Ehd1*), a central promotor in the flowering network, under LD (Nemoto et al. 2016).

Single mutations in *Ghd7* or *8*, *PRR37*, *PRR73* and several *NF-YC* genes accelerate flowering under LD, consistent with their involvement in LD repressor complexes (Xue et al. 2008; Wei et al. 2010; Koo et al. 2013; Gao et al. 2014; Kim et al. 2016; Liang et al. 2021). In plants harboring *ghd7* or *ghd8* mutations and grown under LD, Hd1 is converted from a repressor to an activator of flowering (Du et al. 2017; Zong et al. 2021; Sun et al. 2022). These genetic data support the hypothesis that the switch in Hd1 function depends upon incorporation of Ghd7 and/or Ghd8 into LD repressor complexes. Under SD inductive conditions, transcription of *Ghd8* is low and Ghd7 protein accumulation is prevented by post-transcriptional mechanisms, thus releasing the promoting activity of Hd1 (Zheng et al. 2019). Whether Hd1 forms different complexes under SD remains to be determined.

The targets of Hd1 include *Hd3a* and *RFT1*, encoding for florigenic proteins expressed in phloem companion cells and loaded into sieve elements. Once in the phloematic stream, they can reach the shoot apical meristem (SAM), acting as long-distance, noncell autonomous signals and promoting the transition of the apex from vegetative to reproductive. While several lines of evidence support phloematic expression of Hd3a and RFT1, the question of whether Hd1 expression is limited to the phloem is still unanswered (Tamaki et al. 2007; Komiya et al. 2009; Pasriga et al. 2018) It is equally unknown whether Hd1 has additional targets, either direct or indirect.

In this study, we used genome-wide and biochemical approaches to explore the regulatory landscape of the Hd1 protein.

Results

Mutations in *Hd1* modify the leaf transcriptome more extensively under LD

In Arabidopsis, *CONSTANS* is transcribed in companion cells of the phloem. Its misexpression under the companion cell-specific *SUCROSE TRANSPORTER 2* (*SUC2*) promoter is sufficient to accelerate flowering, whereas misexpression in the SAM does not result in appreciable changes in flowering time (An et al. 2004). In rice, transcription of *Hd1* has not been studied at the tissue-level, although the gene is also assumed to be expressed in vascular tissues, because *Hd3a* and *RFT1* are activated there (Komiya et al. 2008; Pasriga et al. 2018). We stably transformed a *pHd1:GUS* vector previously used in transient assays (Goretti et al. 2017) into Nipponbare, and analyzed GUS expression patterns of independent T2 transgenic plants under LD conditions (Fig. 1, A to D). During early developmental stages, when plants were 3 weeks old, GUS expression was detected in the vascular tissue of the leaf (Fig. 1, A and B). At advanced stages of development, when plants were 6 weeks old, GUS expression was detected in the phloem as well as in all mesophyll cells, but not in the epidermis (Fig. 1, C and D). This pattern is consistent with *Hd1* controlling expression of *Hd3a* and *RFT1* in the vasculature, but also suggests that *Hd1* has a broader expression, and might target additional genes controlling physiological processes other than flowering time.

Following this hypothesis, we performed a global analysis of gene expression by RNA-sequencing, comparing the leaf transcriptomes of *hd1-1* mutants vs. Nipponbare wild type, under both LD and SD. Triplicate samples were collected at *Zeitgeber* 0 (ZT0), 70 and 56 days after sowing in LD and SD, respectively. Flowering time and the expression of known *Hd1* target genes, including *Hd3a* and *RFT1*, were quantified to assess proper growth conditions and transcription patterns. The results were consistent with published data (Supplementary Fig. S1, A to C).

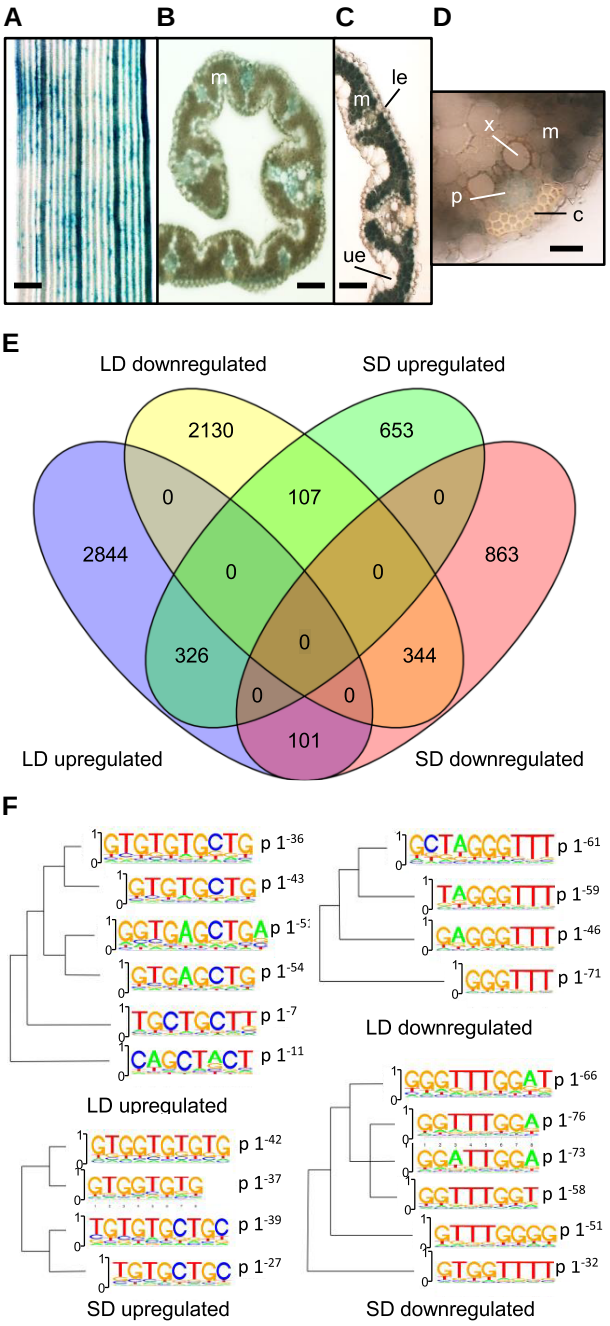

Figure 1. Transcriptional changes caused by *Hd1* in the leaf under LD and SD. A-D, GUS assays on rice leaves transformed with a *pHd1:GUS* vector. **A, B)**, 3-week-old rice leaves showing GUS expression in the vasculature. **C)** 6-week-old leaf showing GUS expression in the mesophyll. **D)** magnification of a 6-week-old vascular bundle showing details of conductive tissues. Scale bars: A = 100 μm, B and C = 50 μm, D = 20 μm; m, mesophyll; le, lower epidermis; ue, upper epidermis; p, phloem; c, collenchyma;×indicates a vessel element cell of the xylem. **E)** Venn diagram summarizing genes differentially expressed in *hd1-1* compared with wild type, under LD and SD at FDR < 0.05. **F)** logo plots of enriched DNA motifs in the promoters of DE genes, filtered for FDR < 0.05 and $\log_2$FC≥|1.5|. Note the enrichment of *TGTG*-containing motifs in genes downregulated in the mutant.

When applying an FDR ≤ 0.05, we identified 5,852 differentially expressed genes (DEGs) between *hd1-1* mutants and wild-type Nipponbare under LD, with a slight over-representation (56%) of upregulated genes (Fig. 1E; Supplementary Tables S1 and S2 report the complete lists of genes from LD and SD experiments, respectively). Under SD, 2,394 genes were differentially expressed, less than half as many as under LD, with a slight over-representation (55%) of downregulated genes. Differences became even more evident when filtering also for fold change. An arbitrary $\log_2$FC≥|1.5| reduced LD DEGs to 2188, and SD DEGs to 81 only. These data indicate that *Hd1* has a greater effect on the transcriptome under LD than under SD.

The abundance of Hd1 protein cycles during the day and is highest during the light phase. The accumulation profile is the result of translation from cycling RNA, as well as protein degradation—mediated by the autophagy pathway—in the dark (Yang et al. 2015; Hu et al. 2022). With the list of LD DEGs filtered by $\log_2$FC≥|1.5|, we used Phaser to determine if specific peak expression phases were enriched among the clock-controlled genes whose expression also depends upon Hd1 (Mockler et al. 2007). The data indicated that, of the cycling genes, those having peak expression at ZT0-1 and ZT4-9 were enriched in the dataset, with respect to random sampling (Supplementary Fig. S1D). These observations are consistent with the hypothesis that mutations in *Hd1* have a stronger impact on genes with peaks of expression occurring during the light.

Next, we compared genes differentially expressed in *hd1* under either LD or SD, with genes whose expression depends upon the shift from long to short day lengths, using datasets in which conditions were very similar (albeit not identical) to those used in this study (Galbiati et al. 2016). The scope of this meta-analysis was to quantify the overlap between the *hd1*- and photoperiod-dependent transcriptomes, and possibly identify overrepresented categories at their intersection. Only 8 genes were in common to the *hd1* SD and photoperiod datasets (but not *hd1* LD), and among them *OsMADS1*, *OsMADS14* and *Hd3a* were identified as being transcribed in response to *Hd1* and under SD (Supplementary Fig. S2). Thus, while short, this list contains genes with physiological roles during the reproductive phase. The function of *OsMADS1* and *OsMADS14* in leaves is still unclear, although the latter is known to be expressed only under SD, with a peak of expression occurring during the night (Brambilla et al. 2017). The overlap between genes regulated by *Hd1* under LD and those controlled by photoperiod consisted of 403 genes. This overlap is highly significant by factor of over-representation (4) and *P*-value ($P < 3.1$ e-136). However, we did not find enriched functional categories within this group. Thus, the LD transcriptome of *hd1* shared similarities with that of SD-treated wild type plants, but no specific pathway or functional category was evident.

Finally, we retrieved the promoters of DEGs spanning −1 kb to +100 bp from the transcriptional start site (TSS) and scanned them with algorithms for de novo discovery of binding sites based on motifs enrichment (see Materials and methods section). Among promoters of DEGs, we identified several motifs statistically supported, both among up and downregulated genes, in both photoperiods (Fig. 1F). Interestingly, promoters of upregulated genes frequently harbored a *TGTG* sequence, which is also present in *FT* and *Hd3a CORE* regions, and essential for binding of CO/NF-Y and Hd1/NF-Y, respectively. Promoters of downregulated genes were enriched with sequences containing *GGTTT*. The difference between enriched motifs did not depend on day length, but on the direction of differential expression, indicating an *Hd1*-dependent effect. This analysis does not demonstrate direct binding of Hd1 to enriched motifs. One possibility is that Hd1 changes preference for DNA, depending on whether it acts as promotor or repressor of transcription. However, it should be noted that, given the reduced depth of the SD transcriptome data, *GGTTT* motifs require further validation.

Genes belonging to the phenylpropanoid pathway are enriched among DEGs in the *hd1* LD transcriptome

Next, we determined enrichment of specific categories by performing Gene Ontology (GO) analyses (Supplementary Fig. S3 shows ontology groups statistically enriched according to the Gene Ontology Resource database, https://geneontology.org). Under LD, we observed several GO terms related to the phenylpropanoid biosynthetic pathway. Many genes encoding enzymes of the pathway were upregulated, consistent with *Hd1* acting as transcriptional repressor (Supplementary Fig. S4). To investigate whether the dual transcriptional effect of *Hd1* applied to genes other than *Hd3a* and *RFT1*, we sought phenylpropanoid pathway genes downregulated in *hd1-1* under SD. Among those that were upregulated under LD and downregulated under SD in the RNA-Seq experiment, we selected *PHENYLALANINE AMMONIA LYASE 4* (*OsPAL4*, LOC_Os02g41680). *CINNAMYL-ALCOHOL DEHYDROGENASE* (*OsCAD8B*, LOC_ Os09g23540) was chosen as example of a gene downregulated under LD, to assess if *Hd1* could also act as LD activator of gene expression. We quantified their transcription during 24 h time course experiments, expanding on the initial single-time settings of RNA-Seq experiments (Fig. 2, A to D). We observed reduction of *OsPAL4* expression in SD, while steady-state mRNA levels increased under LD in *hd1-1* at all time points (Fig. 2, A and C). *OsCAD8B* expression was lower in the mutant under LD, but identical to the wild type under SD, throughout the time course (Fig. 2, B and D).

We next determined patterns of gene expression in a second *hd1* mutant allele from a different rice variety. To this end, we exploited BC3F3 lines obtained from a cross between Nipponbare and Augusto, with Augusto used as recurrent parent (see Materials and methods section). Augusto harbors loss-of-function alleles of *Hd1*, *Ghd7* and *Ghd8*. The Augusto *hd1* allele has a frameshift mutation that disrupts the CCT domain (Gómez-Ariza et al. 2015). We derived all combinations of *hd1*, *ghd7* and *ghd8* mutations in the Augusto background and used 2 introgressions selected to bear $hd1^{AUG}$ $Ghd7^{NB}$ $Ghd8^{NB}$ (hereafter AUG^{hd1}) and $Hd1^{NB}$ $Ghd7^{NB}$ $Ghd8^{NB}$ (hereafter AUG^{Hd1}). As expected, flowering was accelerated in AUG^{hd1} compared with AUG^{Hd1} (Fig. 2E). Expression of *OsPAL4* and *OsCAD8B* was quantified in leaves of plants grown in a field and harvested at the summer solstice when day length was at its maximum (15 h 40 m). *OsPAL4* and *OsCAD8B* transcription showed opposite regulation in AUG^{hd1} compared with AUG^{Hd1}, consistent with data obtained from controlled growth conditions (Fig. 2F).

OsPAL4 is found in a genomic cluster containing 4 *PAL* genes, all of which were upregulated under LD in *hd1-1*, based on RNA-Seq data (Supplementary Table S1). We quantified transcription of *OsPAL1* (LOC_Os02g41630) and *OsPAL2* (LOC_Os02g41650) under LD and SD in *hd1-1* and AUG^{hd1} mutant backgrounds and observed patterns like *OsPAL4* (Fig. 2, G and H). Quantification of *OsPAL3* (LOC_Os02g41670) mRNA expression failed due to amplification of multiple transcripts in qPCR experiments.

These data indicate that *Hd1* has opposite effects on transcription of *OsPAL4*, similar to the regulation of florigens and that it can also operate on genes not belonging to the photoperiodic flowering pathway.

Hd1 binds the promoter of *OsPAL4*

We then used chromatin immunoprecipitation (ChIP) to assess binding of Hd1 to DNA. To this end, we exploited a line overexpressing FLAG-tagged Hd1 under the control of the maize *ACTIN* promoter (*pACT:3xFLAG:Hd1*). Plants harboring this vector

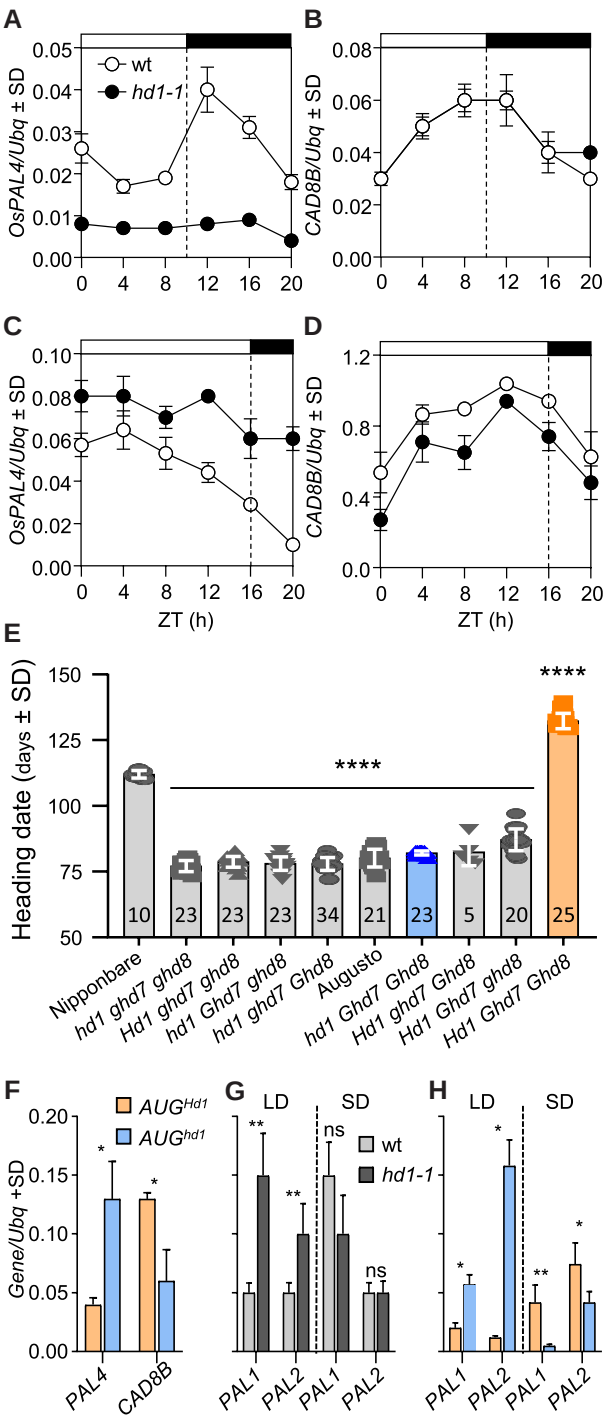

Figure 2. Transcription of genes in the phenylpropanoid pathway. Transcription of *OsPAL4* **A, C)** and *OsCAD8B* **B, D)** quantified under SD **A, B)** and LD **C, D)** in Nipponbare and *hd1-1*. White and black bars on top of the graphs indicate day and night periods, respectively. ZT, *Zeitgeber*. **E)** Flowering time of BC3F3 lines scored under natural LD in Milan. The number of plants scored is indicated in each histogram. Genotypes are indicated on the× x-axis. Blue and orange bars indicate the AUG^{Hd1} and AUG^{hd1} genotypes, respectively. The same color code was used in **F** and **H**. ****$P < 0.0001$ based on ordinary 1-way ANOVA. **F)** quantification of *OsPAL4* and *OsCAD8B* transcription in field-grown plants harvested 4 h after dawn at the summer solstice. **G**, **H**) Quantification of *OsPAL1* and *OsPAL2* transcription in *hd1* mutant alleles under controlled LD and SD. Each quantification in **A** to **D)** and **F** to **H)** represents the average ± standard deviation (SD) of 3 technical replicates. *UBIQUITIN* (*Ubq*) was used to normalize gene expression. Asterisks indicate statistical significance based on Student's *t*-test. *$P < 0.05$; **$P < 0.005$.

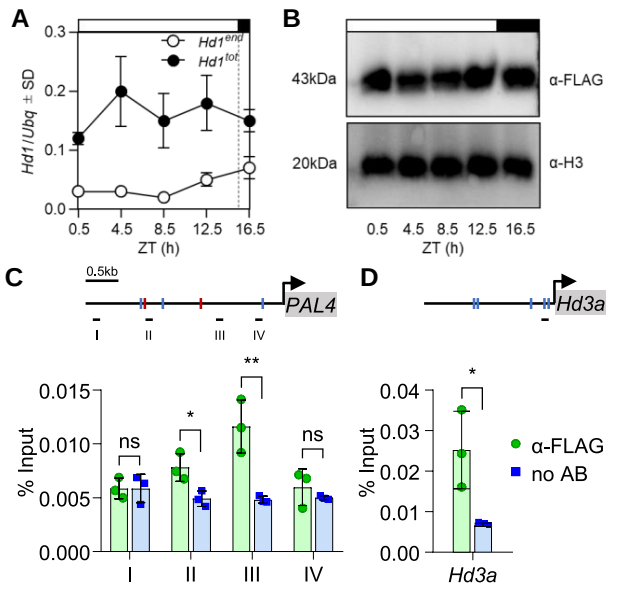

Figure 3. Hd1 binds the *OsPAL4* promoter. Diurnal accumulation profile of endogenous (*Hd1*^{end}) and endogenous + transgenic *Hd1* (*Hd1*^{tot}) mRNA from a time course in leaves under LD **A)** compared with accumulation of 3xFLAG-Hd1 from the same samples. **B)** Western blots were repeated twice with biologically independent samples, giving the same results. Anti-histone H3 was used as loading control. Transcriptional quantifications represent the average ± standard deviation (SD) of 3 technical replicates. *UBIQUITIN* (*Ubq*) was used to normalize gene expression. ZT, *Zeitgeber*. ChIP-qPCR quantifications of Hd1 binding to the promoter regions of *OsPAL4* **C)** and *Hd3a* **D)**. Schemes on top of the graphs indicate the promoter regions. Red and blue marks indicate *TGTGG* motifs on the plus and minus strands, respectively. Black lines below the promoters indicate the position of the amplicons used to quantify fragments enrichment. Each bar represents the average ± standard deviation (SD) of 3 technical replicates. Values are shown relative to the input. ChIP-qPCRs were repeated 4 times independently, giving the same results. Asterisks indicate statistical significance based on Student's *t*-test. *$P < 0.05$; **$P < 0.005$.

produce a FLAG-Hd1 protein of the expected size and flower late under 16.5 h photoperiods (Eguen et al. 2020). We measured FLAG-Hd1 protein abundance at several time points, under the same growth conditions used for the LD RNA-Seq experiment and observed similar accumulation at every time of day tested (Fig. 3B). The protein accumulation pattern followed the transcriptional pattern (Fig. 3A), and no evidence of post-translational control of protein abundance was evident, although it is possible that high protein expression might have masked regulatory layers relevant in a wild type context. Nonetheless, this experiment indicated that the Hd1 protein is stable in vivo, distinct from the situation observed for CO. We used leaves harvested at ZT1 for chromatin preparations. Following IP with anti-FLAG antibodies, we quantified DNA at the *Hd3a* and *OsPAL4* promoters. An amplicon spanning the *OsCORE2* motif in the *Hd3a* promoter was used as a positive control, because the motif has been previously assayed for Hd1 binding in vitro (Goretti et al. 2017). We observed Hd1 binding at the *OsPAL4* locus, in a region spanning several *TGTGG* motifs (Fig. 3, C and D). Therefore, Hd1 directly binds the *OsPAL4* promoter and regulates its transcription, similarly to *Hd3a*.

The leaf proteome is modified by changes in day length

We asked how day length and/or Hd1 might alter the leaf proteome. Therefore, we carried out total leaf proteome analysis in the Nipponbare wild type and *hd1-1* plants under both SD and LD conditions. Triplicate samples were collected at ZT0 for each condition. Leaves were harvested 30 days after sowing (LD) and after 15 additional days of growth under SD. Mass spectrometry was performed for untargeted proteomics. A total of 6,186 proteins were identified. Comparisons between photoperiods showed that 283 were significantly enriched under LD and 311 were significantly enriched under SD conditions in the wild type. In the *hd1-1* mutant, the equivalent numbers were 474 under LD and 462 under SD conditions (Supplementary Figs. S5 and Table S3). Comparisons between genotypes under the same photoperiodic conditions showed negligible differences under SDs (1 protein more abundant in the wild type and 1 in *hd1-1*). Under LD conditions, 19 proteins were more abundant in the wild type and 12 in the *hd1-1* mutant. We attribute these marginal differences between genotypes to the depth of total proteome analyses, which likely capture only major differences. Nevertheless, these data indicate that changes in daylength have a prominent effect on the leaf proteome, and that changes during the photoperiodic transition are accentuated by the *hd1* mutation. Analysis of ontological categories indicated that changes in day length affected several metabolic processes. On the contrary, comparison between wt and *hd1-1* under LD conditions identified only GO terms related to cell wall metabolism (Supplementary Fig. S6).

Mutations in *Hd1* modify cell wall composition

Both RNA and protein profiling suggest that Hd1 could affect cell wall composition and biogenesis. Therefore, we performed a more detailed biochemical characterization. To this end, we extracted cell wall polymers from the alcohol insoluble residue (AIR) of *hd1-1* and wild type, using either 50 mM cyclohexane-1,2-diaminetetraacetic acid (CDTA) or 4 M sodium hydroxide (NaOH). CDTA at relatively low concentration solubilizes polymers with weak association to the cell wall, whereas NaOH solubilizes polymers strongly attached to it (Ezquer et al. 2016). We will refer to the CDTA and NaOH extractions as soft and harsh, respectively. Quantifications were performed by enzyme-linked immunosorbent assay (ELISA), using the set of antibodies listed in Supplementary Table S4.

Pectins are typically soluble in water or CDTA. However, the harsh treatment released extra material that was not extracted with the soft treatment. In the soft extract, *hd1-1* exhibited significantly lower signals for the backbone of rhamnogalacturonan I (RG-I, backbone of alternating galacturonic acid and rhamnose and typical side chains consisting of arabinose and galactose; $P < 0.01$) and unesterified homogalacturonan (HG, linear chain of galacturonic acid to which methyl or acetyl groups can be attached; $P < 0.05$) when compared with the wild type (Fig. 4, A and C). In contrast, in the harsh extract, *hd1-1* showed increased abundance of both RG-I side chains, β-1-4-galactan ($P < 0.01$) and α-1-5-galactan ($P < 0.01$) (Fig. 4, B and D). These data suggest that pectins belonging to the RG-I group are more ramified in the *hd1-1* mutant.

Arabinogalactan-proteins are highly glycosylated proteins integral to plant cell walls and involved in many activities related to cell growth and development. We used 5 antibodies to profile AGPs of cell wall preparations. In the soft extract, *hd1-1* showed lower abundance of AGPs detected by JIM13 (recognizing carbohydrate residues of AGPs located on the outer surface of the plasma membrane; $P < 0.05$, Fig. 4E). In the harsh extraction, JIM8 and JIM13 produced stronger signals in the *hd1-1* mutant compared with the wild type (Fig. 4F). JIM8 has similar properties as JIM13,

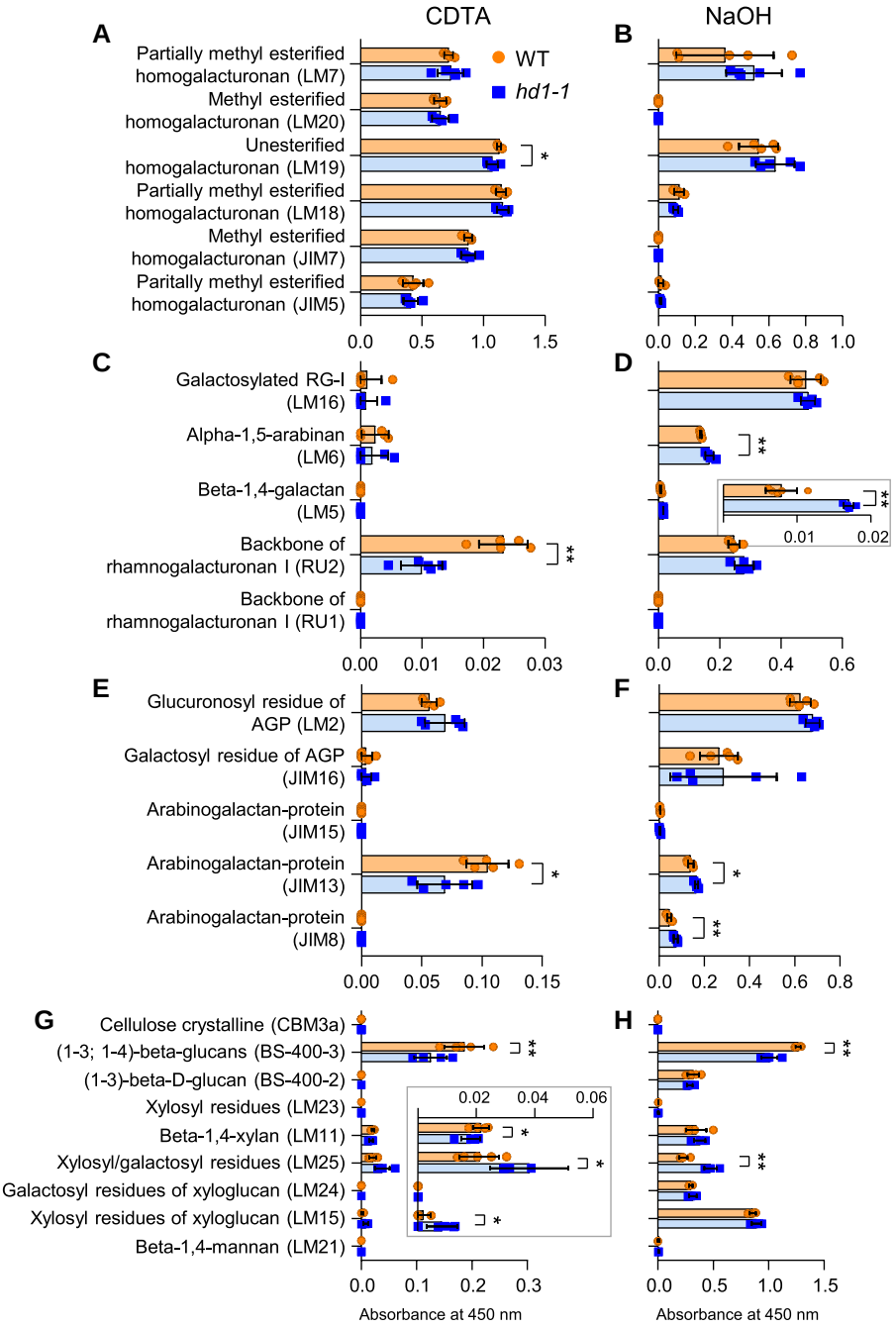

Figure 4. Cell wall composition of the *hd1* mutant. **A, C, E, G)** Quantifications of loosely adhered components (CDTA extractions). **B, D, F, H)** Quantifications of strongly adhered components (NaOH extractions). **A** to **D**) Quantifications of pectins. Histograms are divided into 2 groups **A, C** and **B, D)** to facilitate reading, because of the different scales of values. Inset in **D)** magnifies the corresponding beta-1,4-galactan values. **E**, **F**) Quantifications of arabinogalactan proteins. **G**, **H)** Quantifications of crystalline cellulose and hemicellulose. Inset in **G)** magnifies the corresponding beta-1,4-xylan, xylosyl/galactosyl residues and xylosyl residues of xyloglucan values. Bars indicate the average ± standard deviation of 5 biological replicates, except for beta-1,4-mannan values where 3 and 4 replicates were used for *hd1-1* and wt, respectively. Each dot represents an independent sample. Asterisks indicate statistical significance based on 2-tailed Student's *t*-test. *$P < 0.05$; **$P < 0.01$.

but it immunoreacts with less AGPs. This may indicate that AGPs that strongly adhere to the extracellular matrix are more prevalent in the mutant. However, given the large number of secreted AGPs and their polymorphisms, this conclusion requires further support.

The fibrillar component of the cell wall was assayed using antibodies marking cellulose as well as some epitopes for hemicellulose. The *hd1-1* mutant had lower levels of (1-3; 1-4)-β-glucans in both the CDTA ($P < 0.01$; Fig. 4G) and NaOH ($P < 0.01$; Fig. 4H) extractions. Lower signal intensities were also detected for β-(1-4)-xylan, although only in soft extractions and at marginal statistical significance ($P < 0.05$; Fig. 4G). Xyloglucans are composed of variable building blocks, formed by linear glucans to which xylosyl and galactose units can be added. Building blocks made of 4 glucosyl units, α1,6-linked to 3 xylosyl units, are indicated as XXXG. in turn, xylosyl units can be β1,2-linked to 1 or 2 galactose units, and are indicated as XXLG and XLLG, respectively. The *hd1-1* mutant showed higher levels of xylosyl/galactosyl residues (XXLG and XLLG motifs) both in the soft ($P < 0.05$; Fig. 4G) and harsh ($P < 0.01$; Fig. 4H) extractions. It also showed higher

levels of XXXG motifs, detected by LM15, but only in CDTA extractions at $P < 0.05$ (Fig. 4G). These data indicate that *hd1* mutations alter the fibrillar component of leaves cell walls, reducing (1-3; 1-4)-β-glucans and β-(1-4)-xylan, while increasing xyloglucans of the XXLG and XLLG types.

Finally, we quantified the acid-soluble as well as the acid-insoluble fractions of lignin, following Sluiter et al. (Sluiter et al. 2004). Both fractions were lower in the *hd1-1* mutant, with the acid-insoluble lignin being more significantly reduced (Fig. 5A). These quantifications were repeated also in the *hd1-2* mutant, showing similar patterns (Fig. 5A). Cell wall staining followed by imaging did not reveal obvious morphological alterations at tissue or cell levels (Fig. 5, B to E).

Mutations in *Hd1* change salt stress tolerance in a photoperiod-dependent manner

The results presented so far indicate that *Hd1* could have broader roles than the control of flowering time and affect other physiological processes. We hypothesized that abiotic stress tolerance might be altered in the mutant, also considering that GO categories suggested involvement in response to external stimuli and to abscisic acid—a stress hormone—detoxification of reactive oxygen species and general defense responses (Supplementary Fig. S3). We choose salinity stress to challenge this hypothesis. We grew wild type and *hd1* mutants in artificial media containing 300 mM sodium chloride, and measured shoot growth as proxy of salt sensitivity, calculating an index based on comparison between treated and nontreated plants (see Materials and methods section). We observed that salt sensitivity did not change in the wild type grown under different day lengths. However, in *hd1-1* and *hd1-2* mutant alleles, salt sensitivity diverged depending on the photoperiod, increasing under LD and decreasing under SD (Fig. 6, A to C). Thus, despite no statistically significant difference was observed between wild type and mutant plants grown in the same photoperiod, salt stress was perceived differently by *hd1* mutant plants grown in LD and SD. We assayed *pACT:3xFLAG:Hd1* and observed no difference between photoperiods, but significant reduction of sensitivity compared with *hd1* mutants under LD (Fig. 6C). In Augusto, salt sensitivity was less variable compared with Nipponbare, in which ample variability was evident, particularly under SD (Fig. 6D). Yet, also in this variety, the AUG^{hd1} genotype showed differential sensitivity to salt stress, depending on day length. Finally, we assayed an introgression harboring $Hd1^{NB}$ $ghd7^{AUG}$ $ghd8^{AUG}$ (hereafter $AUG^{ghd7,8}$), whose flowering time was very similar to that of AUG^{hd1}, having loss-of-function alleles of *Ghd7* and *Ghd8* LD repressors (Fig. 2E). Salt sensitivity of $AUG^{ghd7,8}$ diverged similarly to *hd1* mutants across photoperiods, despite marginal statistical significance (Fig. 6D). Taken together, these data indicate that rice plants respond differently to salt stress, depending on the photoperiod, but only in genetic backgrounds in which LD floral repression is relaxed.

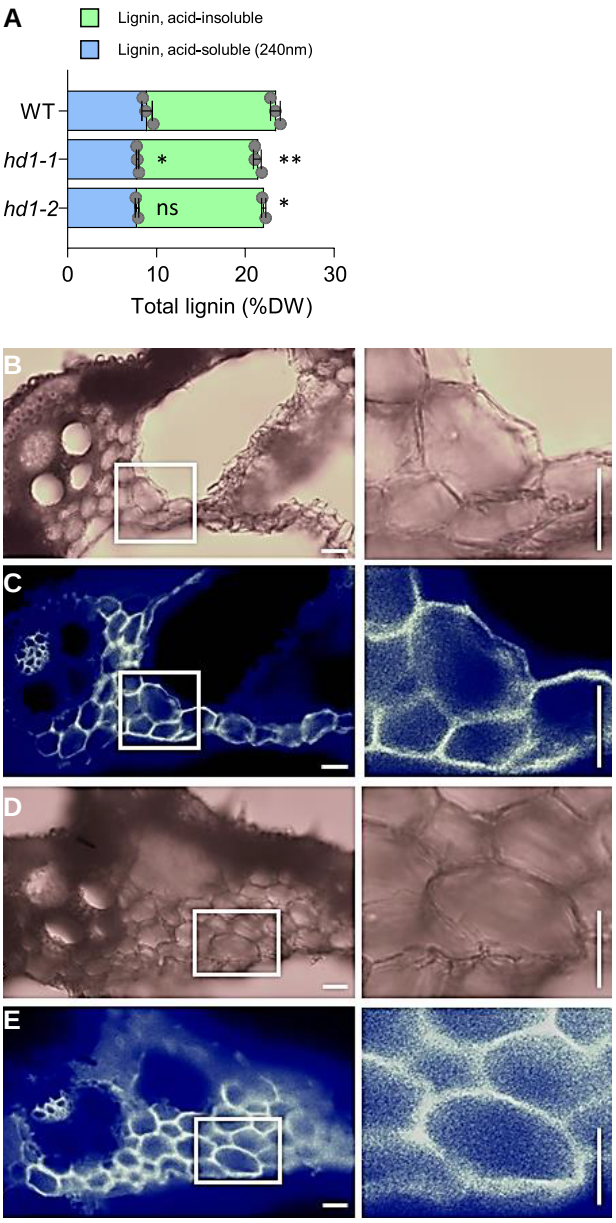

Figure 5. Lignin content and cell morphology of *hd1-1* mutants. **A)** lignin content expressed as % of dry weight (DW) in Nipponbare wild type, *hd1-1* and *hd1-2* mutant leaves grown under LD for 70 days. Each dot represents a biologically independent sample. Error bars indicate the standard deviation. Asterisks indicate statistical significance based on 2-tailed Student's *t*-test. *$P < 0.05$; **$P < 0.01$; ns, nonsignificant. **B** to **E**) Cell wall stainings in *hd1-1* and WT leaf sections in 70-day-old plants. **B**, **C)** SCRI Renaissance 2200 (SR2000) staining of the *hd1-1* central vein section captured in transmitted light **B)** and with DAPI filter **C)**. **D**, **E)** SR2000 staining of the WT central vein section captured in transmitted light **D)** and with DAPI filter **E)**. Magnifications on the right show parenchyma cells details of the areas framed on the left. Scale bars, 20 μm.

Discussion

Plants experience continuous changes in day length, even at latitudes close to the equator, and have adapted to anticipate and respond to them. Flowering time is very susceptible to such changes, and observation of the flowering behavior of certain species has been instrumental to the recognition of photoperiod measurement systems (Garner and Allard 1920). However, recent studies have demonstrated that changes in photoperiod can influence several processes unrelated to flowering, including bud dormancy in trees, tuber or bulb formation, and growth, to mention a few important examples (Lee et al. 2013; Abelenda et al. 2016; Tylewicz et al. 2018; Wang et al. 2024). Thus, the photoperiodic pathway, originally and commonly studied in the context of flowering, can be integrated in broader response systems. In rice, Hd1 is central in the photoperiodic flowering pathway and when mutated, alters the capacity of the plant to correctly perceive seasonal

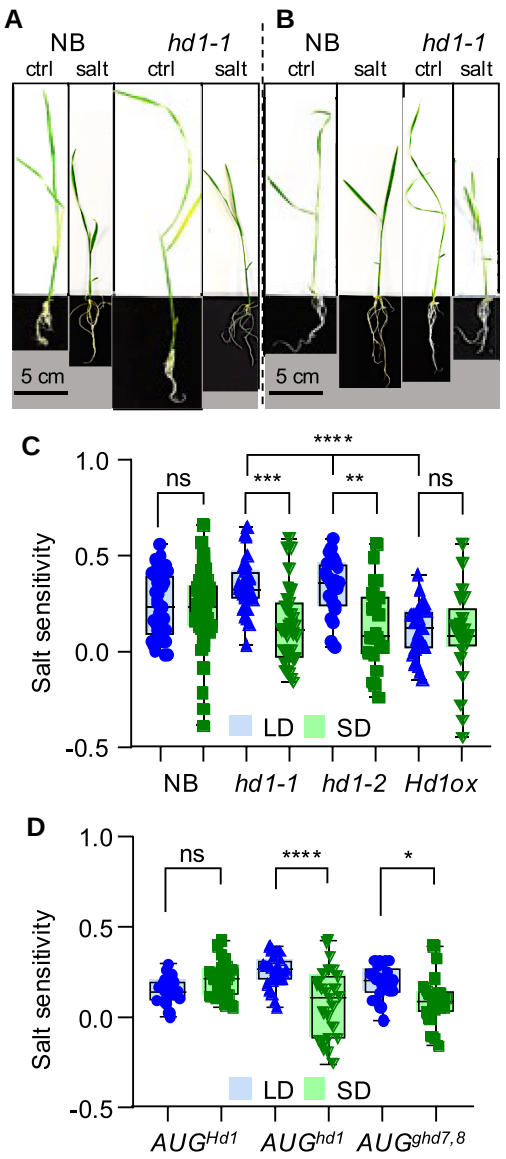

Figure 6. Salt stress assays in *hd1* mutants. **A**, **B)** Representative pictures of WT and *hd1-1* mutant seedlings grown in MS media with and without salt, under LD **A)** or SD **B)**. **C)** Box plots showing salt sensitivity of Nipponbare, *hd1-1*, *hd1-2* and *pACT:3xFLAG:Hd1* (*Hd1ox*). **D)** Box plots showing salt sensitivity of Augusto introgression lines. Each box indicates the 25th–75th percentiles, the central line indicates the median and the whiskers indicate the full data range. Each dot indicates a pair of plants (control and treated) used to calculate the index. Pairs of measurements were randomly sampled and used only once. $^{*}P < 0.05$; $^{**}P < 0.005$; $^{***}P < 0.0005$; $^{****}P < 0.0001$, ns, nonsignificant based on ordinary 1-way ANOVA. The experiment was repeated 3 times independently, with similar results.

changes and flower at the correct time of the year. The data presented in this study, extend the roles of Hd1 and suggest that it has a broader impact on plant physiology.

Cell wall remodeling in the *hd1* mutant

We have found links between *Hd1* and genes controlling secondary metabolism and cell wall biogenesis, under LD. This observation could be interpreted by postulating either a direct effect of Hd1 on these pathways, or an indirect effect caused by reduced day length sensitivity of the *hd1* mutant. Binding of Hd1 to the promoter of *OsPAL4* supports the former hypothesis, but both could be valid, and more thorough analyses are required to distinguish between them. Nevertheless, quantification of cell wall polymers detected differences between wt and mutant, allowing to draw conclusions on the role of Hd1 in cell wall remodeling.

The cell wall is a highly organized structure enclosing every plant cell, and formed by polysaccharides, proteins and phenolic compounds (Cosgrove 2024). Polysaccharides include cellulose, hemicellulose and pectin. Cellulose is a homopolymer of β-(1,4)-D-glucose, and the main component of primary walls. Hemicellulose includes a heterogenous group of polysaccharides formed by a backbone of 1,4-beta-linked sugars, to which side chains of 1 to 3 sugar residues are covalently linked. The most common hemicellulose of flowering plants is xyloglucan (XyG). However, the cell wall of grasses contains small amounts of XyG, and the most abundant hemicellulose is arabinoxylan. Pectin is found mainly on the outer side of the wall, in the middle lamella, working as a glue between cells. The building block of pectin is α-(1-4)-D-galacturonic acid, forming homopolymers (homogalacturonan) or heteropolymers of rhamnose and galacturonan (RG-I). Homogalacturonan can also present rhamnogalacturonan side chains (RG-II), as well as xylose or other monosaccharide substitutions.

Cellulose is polymerized by CELLULOSE SYNTHASEs, that reside on the plasma membrane and are organized in multimeric cellulose synthase complexes (CSCs). Cellulose biosynthesis follows diurnal oscillations depending on light and carbon availability, but not on the circadian clock (Ivakov et al. 2017). Seasonal photoperiodic patterns in cellulose biosynthesis have also been observed. In Arabidopsis, the blue-light photoreceptor FLAVIN-BINDING KELCH REPEAT, F-BOX 1 (FKF1) stabilizes CO to promote flowering under LD, while inhibiting cellulose biosynthesis in the leaves (Yuan et al. 2019), providing direct evidence of the connection between the photoperiod pathway and cellulose production.

Both extraction profiles indicated that *hd1* contains less (1-3; 1-4)-beta-glucans and more xylosyl residues of XyG (especially XXLG and XLLG types) in mature leaves. Since the (1-4)-beta-glucan backbone is common to both cellulose and XyG, these data suggest that in *hd1* cellulose is less abundant, XyG are shorter and more ramified, or both. In wt rice, *OsCESA3* and *6* are ubiquitously expressed and are necessary to synthetize microfibrils in primary walls. Expression of *OsCESA4*, *7* and *9* has also been detected in most rice tissues at relatively high levels, with the notable exception of mature leaves, in which transcript abundance is very low or undetectable (Tanaka et al. 2003; Wang et al. 2010). Among the DEGs, *OsCESA1*, *4*, *6*, *7*, *9* and several *OsCESA LIKE* (*CSL*) genes were upregulated in *hd1* under LD. Thus, the accumulation profiles of (1-3; 1-4)-beta-glucans and *OsCESA/CSL* transcripts were negatively correlated. This suggests that the differences between wt and *hd1* are mostly due to XyG abundance or that layers of post-transcriptional regulation alter the linear relationship between transcript abundance and cellulose production. For example, interaction between OsCESA subunits forming a functional CSC, transport to the plasma membrane, protein phosphorylation or turnover, may affect the final quantity of cellulose produced.

Among the DEGs, we observed higher expression of some *OsCSL* genes belonging to group C (*OsCSLC*). In Arabidopsis, a quintuple mutant lacking all *AtCSLCs*, could not produce XyG (Kim et al. 2020). This observation suggests that among the *OsCSLCs* upregulated in *hd1*, some might contribute to synthetize XyG, rather than cellulose. Distinguishing between these possibilities will require protein localization studies, since cellulose and XyG biosynthetic

enzymes reside on the plasma membrane and on the Golgi membranes, respectively (Cosgrove 2024). We exclude the possibility of compensatory effects between cellulose and XyG production, i.e. an increase of XyG caused by reduction of cellulose. Such hypothesis has already been tested and discarded by Kim et al., who showed that plants lacking XyG have normal cellulose content (Kim et al. 2020).

Xylosylation of the glucan backbone is carried out by glycosyltransferases (GTs). We identified several GTs, all of which were upregulated in *hd1* under LD, and partially overlapped with differentially enriched proteins in the proteomic dataset (LOC_Os06g48180; LOC_Os11g18730). These transcriptional profiles are compatible with the hypothesis that *hd1* harbors more ramified XyG in its cell walls. Therefore, Hd1 contributes to cell wall composition in mature leaves. Further studies are needed to understand the implications of this observation on cell wall stiffness and overall plant development.

Interaction between abiotic stress sensitivity and day length perception

Rice plants are exposed to several abiotic stresses, some of which are exacerbated by climate change, including drought, flooding and exposure to salinity. The latter is particularly relevant in river deltas, where water returning from the sea can intrude for several kilometers in coastal areas. Incorrect water management and fertilizer use also cause soil salinization. Under conditions of high salinity, rice physiology is disturbed by alterations in the osmotic potential, membrane damage, pH instability, as well as the direct toxicity of ions such as Na^+. Excess salt also reduces photosynthetic efficiency and growth, causes wilting and in severe cases, plant death. The response to salinity is integrated in a global defense system, monitoring environmental and endogenous information, to maximize fitness. Thus, it is unsurprising that part of this system incorporates elements of the photoperiodic response network, which is central in plant adaptation, both in natural and artificial environments. However, how these different pathways communicate with each other remains poorly understood, particularly given the unexpected observation that salinity responses are stabilized across photoperiods by components of the flowering network, and genotypes missing such components, most prominently *Hd1*, respond differently to salt depending on day length.

The closest parallel that we can draw is with drought escape (DE) in Arabidopsis, that is a system better characterized at the molecular level. The DE response allows Arabidopsis to flower early if exposed to water deprivation regimes. This adaptation shortens the life cycle, inducing quick seed set (and paying a tradeoff in seed number), if conditions become unfavorable. The trait is photoperiod-dependent, as it occurs under LD, but not SD, conditions. Thus, DE as phenotypic consequence of drought stress, shows differential sensitivity to the photoperiod, similarly to the case of shoot length reported here. Genes within the flowering network, including *GIGANTEA* (*GI*), *FT* and *TWIN SISTER OF FT* (*TSF*) promote the DE response, and plants mutated in these genes flower late, irrespective of watering or photoperiodic conditions (Riboni et al. 2013). This scenario is analogous to rice plants carrying mutations in *Hd1* and exposed to salt, with the notable difference that *Hd1* stabilizes the response in LD and SD, rather than differentiating it.

Drought and other abiotic stresses cause increased production of ABA, in turn coordinating physiological responses, such as stomatal closure, scavenging of reactive oxygen species and osmolyte accumulation (Liu et al. 2022). ABA promotes GI and CO protein activities to induce *FT* transcription in the leaves, resulting in DE (Riboni et al. 2016). Therefore, a plausible interpretation of our findings might be that rice plants exposed to salt stress use Hd1 downstream of ABA signaling to coordinate the responses, in different photoperiods, and that mutations in *Hd1* uncouple day length perception and stress responses. Several lines of evidence support this connection. At the global transcriptional level, it is well established that stress response genes are controlled by the circadian clock, both in Arabidopsis (Covington et al. 2008) and rice (Wei et al. 2022). Altering time measurement by mutating clock genes, prevents proper photoperiodic responses and reduces stress resistance (Wei et al. 2022). Hd1 could be a hub for integration of clock activity and stress responses. If so, more specific hypotheses could be assayed. For example, Arabidopsis PRR proteins, which are integral components of the clock, interact with and stabilize CO during the light phase (Hayama et al. 2017). Triple *prr5 prr7 prr9* mutants have higher tolerance to several stresses, including high salinity, coupled with lower levels of CO protein (Nakamichi et al. 2009). In rice, a clock-dependent mechanism might modify stress sensitivity in the photoperiod, directly as well as indirectly by modifying Hd1 post-translationally. While in Arabidopsis CO protein stability is key to confer a photoperiodic response, Hd1 function is only marginally dependent on its stability, and protein accumulation largely follows transcriptional patterns. Yet, most layers of post-translational protein processing are still to be studied, including phosphorylation or higher order complex formation. We believe the latter could impact on stress tolerance. A homolog of Arabidopsis *PRRs*, *OsPRR73*, is induced by salt stress. If mutated, it increases sensitivity to salt under SD and promotes flowering under LD (Liang et al. 2021; Wei et al. 2021). Importantly, OsPRR73 can form NF-Y complexes, substituting or cooperating with Hd1 to bind DNA. Therefore, Hd1 could be an integrator, downstream of clock-dependent stress responses, or directly involved in controlling expression of stress responsive genes via higher-order complex formation.

Materials and methods

Plant material and growth conditions

Rice (*Oryza sativa*) plants of the Nipponbare and Augusto varieties were used. Augusto carries loss-of-function alleles of *Hd1*, *Ghd7* and *Ghd8*. BC3F3 seeds were obtained by using Augusto as recurrent parental from a Nipponbare × Augusto cross and selecting lines heterozygous for the loss-of-function alleles at each generation. After 3 rounds of backcrossing, plants were allowed to self-fertilize and in the resulting BC3F2 progeny we selected combinations of homozygous loss-of-function and wild type alleles. The null mutants *hd1-1* and *hd1-2* carry the insertion of a *Tos17* retrotransposon in the first and second exon of *Hd1*, respectively, as described in Gómez-Ariza et al. 2015. The *pACT::3xFLAG:Hd1* plants were obtained in the Nipponbare background and are described in Eguen et al. 2020. The *pHd1:GUS* construct contains the functional Nipponbare *Hd1* promoter and is the same used in Goretti et al. 2017.

Plants were grown in phytotrons (Conviron PGR15) at 28 °C and 70% relative humidity (RU) during the day and 24 °C and 90% RU during the night. Photoperiods were set at 16 h light in LD and 10 h light in SD. Propagation of plant materials was done in greenhouses at the Botanical Garden Città Studi. Crosses between Nipponbare and Augusto and flowering time experiments of

BC3F3 families were done under natural LD field conditions at the Botanical Garden Città Studi in Milan.

Quantification of mRNA expression and GUS assays

Total RNA was extracted from 1 g of ground leaves powder using nucleoZOL (Macherey Nagel) and treated with Turbo DNAse (Thermofisher Scientific) to remove residual DNA. One microgram of total RNA was retrotranscribed with the ImProm-II Reverse Transcriptase (Promega) using an oligo dT primer and following manufacturer's instructions. Reverse transcription quantitative polymerase chain reaction (RT-qPCR) was used to quantify transcription of individual genes in an Eppendorf Real Plex2. The list of primers is provided in Supplementary Table S5.

For GUS assays, leaf samples expressing the *pHd1:GUS* construct were fixed in 90% acetone for 20 min on ice, kept under vacuum for 1 h, and then incubated in an X-Gluc solution at 37 °C for 1 h (Jefferson et al. 1987). Subsequently, green tissues were cleared in methanol/acetic acid (3:1, v/v) for 4 h at room temperature, with constant agitation, followed by multiple washes (at least 4) in 70% ethanol. At least 2 independent transgenic lines were used, and the experiment was repeated 3 times with identical results.

Protein preparation and western blotting

Total proteins were extracted from cold-grinded nitrogen-frozen rice leaves placed in extraction buffer (4 M Urea, 50 mM Tris-HCl, 2 mM EDTA, 150 mM NaCl, 0,2% 2-mercaptoethanol, 0,1% SDS and Pierce Protease Inhibitors (Thermo Scientific)). The resulting mixture was centrifuged at 14.000 rpm for 30 min at 4 °C to pellet cell debris, and the supernatant recollected. Total protein concentration was quantified using Quick Start Bradford 1× Dye Reagent (Bio-Rad). Freshly collected protein extracts were then normalized to 60 μg, added with 2× Laemmli sample buffer and loaded on a 10% acrylamide/bis-acrylamide gel (29:1 ratio). Proteins were separated via electrophoresis at a fixed current of 30 mA for 1 h 30 m. Following electrophoresis, proteins were transferred on a methanol-activated PVDF membrane via wet blotting in Tris-Glycine buffer at a fixed current of 45 mA for 1 h. Western blotting was performed by using an anti-Flag (Merck) monoclonal antibody at a 1:1,000 dilution and hybridized overnight at 4 °C. Following washes, a goat anti-mouse-HRP secondary antibody (Bio-Rad) was incubated at 1:10,000 dilution for 1 h at room temperature. The membrane was subsequently developed by using an ECL substrate (Clarity Max, Bio-Rad) and a ChemiDoc (Bio-Rad) Imaging system.

Chromatin immunoprecipitation

ChIP was performed using 5 g of ground tissue powder as previously described, with minor modifications (Perrella et al. 2024). For each experiment, leaves from each genotype were used to extract chromatin. A Bioruptor (Diagenode) was used to shear the chromatin using 40 cycles, each consisting of 30 s on and 30 s off, at high power. Anti-Flag magnetic beads (Sigma-Aldrich M8823) were used to immunoprecipitate chromatin. ChIP-qPCR was performed with a 3 min initial denaturation at 95 °C followed by 40 cycles at 95 °C, 3 s and 59.5 °C, 30 s. Primers are listed in Supplementary Table S5. Reactions were performed on 4 technical replicates and 3 independent biological replicates. Relative enrichment was calculated according to Shapulatov et al. (2023).

Promoters were defined as genomic regions spanning from −1 kb upstream, to 100 bp downstream of transcription start sites (TSS) of rice gene models according to Release 7 of the IRGSP annotation of the reference O. sativa Nipponbare genome assembly (Kawahara et al. 2013) (http://rice.uga.edu/). De novo motif discovery was performed with Weeder 2.0 using the default parameters and conceptual representations of promoter sequences described above. PScan was used to generate *P*-values for the enrichment of motif PWMs generated by Weeder, scanning the same 1 kb intervals upstream of IRGSP v7 TSSs (Pavesi et al. 2004; Zambelli et al. 2009).

Quantification of cell wall components

Generation of AIR

Leaves of the *hd1-1* mutant and Nipponbare wild type were collected at the same age as for RNA-Seq profiling. The central portion of a mature adult leaf was sampled from 10 plants to produce each biological replicate and ground to powder in liquid nitrogen. The AIR extraction was done following the protocol described by Moore et al. (2020). Briefly, the powders were made up to 80% using precooled ethanol in 50 mL tubes and boiled for 15 min to denature any potential cell-modifying enzymes. A destarching step was done with an enzymatic mixture containing amylase and amyloglucosidase from Megazyme (Wicklow, Ireland). Samples were centrifuged at 2500 × *g* for 10 min and the supernatant was discarded. Absolute methanol was added to the pellets at 1:10 (w/v) and the tubes were placed on a tube-rotating wheel for 2 h. After centrifugation at 2500 × *g* for 10 min the supernatant was discarded. The solvent washing was repeated using equal parts of methanol and chloroform, chloroform, equal parts of chloroform and acetone, and lastly acetone. After the acetone was discarded, excess liquid was allowed to evaporate in the fume hood without letting the pellets dry. The pellets were resuspended in ice-cold deionized water and frozen in liquid nitrogen.

Cell wall extraction

The extraction of polymeric material from leaf AIR was performed following a modified protocol from Sathitnaitham et al. (2021). Two extractions were performed using CDTA and NaOH in order to solubilize polymers with varying degrees of association with the cell wall. CDTA was used to solubilize polymers with weak associations to the cell wall (e.g. pectin), while NaOH was used to solubilize more strongly associating polymers (e.g. hemicellulose). For each extraction, 10 mg AIR was weighed into microcentrifuge tubes, and 30 μL of CDTA buffer (50 mM CDTA; 50 mM Tris; pH 7) were added per milligram of AIR. To facilitate efficient mixing, a small stainless-steel ball was introduced into each tube. The tubes were then subjected to mechanical agitation on a Retch Mixer Mill, initially for 2 min at 30 Hz, followed by 2 h at 7 Hz. After extraction, the tubes were centrifuged at 10,000 RPM and the supernatant was stored at −20 °C for subsequent analysis. Immediately thereafter, an extraction with NaOH (4 M supplemented with 0.1% NaBH4) was performed, using the same volume and protocol as the preceding CDTA extraction.

Enzyme-linked immunosorbent assay

ELISA was conducted on plant cell wall AIR using tissue-culture-treated 96-well plates (Costar 3598, Corning, New York, USA), following the protocol outlined by Sathitnaitham et al. Preliminary tests were conducted to determine an optimal concentration for all rice cell wall extracts to be tested. Appropriately diluted 50 μL aliquots of both CDTA and NaOH extracts were dispensed into the 96-well plates and incubated overnight at 37 °C, uncovered. Once the wells were dry, 200 μL blocking agent (3% bovine serum albumin [BSA] in phosphate-buffered saline [PBS]) was added per well, after which the plate was incubated at 37 °C for

1 h and the BSA/PBS was discarded. Each tested antibody was diluted 1:60 in a solution of 1% BSA in PBS, of which 30 μL was used to probe each well. The samples were incubated at 37 °C for 1 h and washed 3 times with PBS. A secondary horseradish peroxidase-conjugated antibody corresponding to each primary antibody was diluted 1:10,000 in 1% BSA in PBS, of which 50 μL was added to each well. A final incubation at 37 °C for 1 h was followed by 6 washes with PBS. 75 μL of freshly prepared chromogenic substrate (3,3′,5,5′-tetramethylbenzidine at 0.42 mM) was added to each well and the resulting colour-forming reaction was allowed to proceed for 30 min before being stopped by the addition of 125 μL sulfuric acid (1 M). Absorbance values were quantified at 450 nm using a Multiskan GO Microplate Spectrophotometer (Thermo Fisher Scientific, Inc., Waltham, MA, USA). Antibodies are listed in Supplementary Table S4.

Lignin quantifications were performed at Measurlabs (Finland) according to the National Renewable Energy Laboratory (NREL) standards (https://www.nrel.gov/docs/gen/fy13/42618.pdf).

Cell wall staining

Leaf portions of about 1 cm^2 were collected from the mid apical region of mature rice leaves of WT, *hd1-1* rice plants grown in LD conditions for 70 days. Chlorophyl was removed from leaf samples by ethanol series and hand-made sections were performed under a stereomicroscope (Zeiss™). Sections were subsequently stained for 1 h at room temperature in the dark with a 1:2,000 dilution of SCRI Renaissance 2200 (SR2200, Renaissance Chemicals), a fluorescent dye (EX 350, EM 415/476) that specifically labels cell walls (Musielak et al. 2015). A 20′ washing step in water was then added to remove staining solution in excess. Sections were mounted in water and visualized with an Axio Imager M2 Fluorescence microscope (ZeissTM) using a DAPI filter (EX 365/10, DM 395 LP, EM BP 445/50). Fluorescent images were taken with the same settings by using either a 5X or a 20X objective.

Salinity stress assays

The effect of salt stress was analyzed in plants grown in vitro. Seeds were surface sterilized (1 wash in ethanol 70% for 1 min, followed by 15 min of wash in commercial bleach and 4 washes of 10 min each with sterile, distilled water), and placed in culture boxes containing 50 mL of solid growth medium (basal medium Murashige and Skoog with vitamins M0222 Duchefa 4.4 g/L, sucrose 30 g/L, Plant Agar P1001 Duchefa 5 g/L). Ten seeds were germinated in each box. Seven days after germination, 50 mL of liquid medium (same as solid medium, but without Plant Agar) was added in control boxes, and 50 mL of liquid medium supplemented with 300 mM NaCl was added to induce salt stress. Pictures of control and treated plants were taken 14 days after germination and shoot length was measured using ImageJ (https://imagej.net/ij/). The salt sensitivity index was calculated as (shoot length control—shoot length treated)/shoot length control. Control and treated plant pairs were randomly chosen.

Proteomic analysis

Protein extraction

Rice leaves were frozen in liquid nitrogen immediately after sampling, and total proteins were extracted with a pH neutral buffer (4 M Urea; 50 mM Tris-HCl pH 7.5; 150 mM NaCl; 2 mM EDTA; 0,2% 2-mercaptoethanol; 0,1% SDS; Pierce Protease Inhibitor by Thermo Scientific). Protein content was quantified by Quick Start Bradford 1× Dye Reagent (Bio-Rad). Mass spectrometry was performed at the EMBL Proteomics Core Facility in Heidelberg—Germany (https://www.embl.org/groups/proteomics), as described below.

Sample preparation

Samples were prepared using the SP3 protocol on a KingFisher APEX system (ThermoFisher Scientific) essentially as described in Leutert et al. (Leutert et al. 2019). Peptides were eluted off the Sera-Mag Speed Beads (GE Healthcare) by tryptic digest (sequencing grade, Promega) in an enzyme to protein ratio 1:50 for overnight digestion at 37 °C (50 mM HEPES, pH 8.5; 5 mM Tris(2-carboxyethyl) phosphinhydrochlorid; 20 mM 2-chloroacetamide). Peptides were labeled with Isobaric Label Reagent (Thermo Scientific) according to the manufacturer's instructions, combined and desalted on an OASIS HLB μElution Plate (Waters). Offline high-pH reverse phase fractionation was carried out on an Agilent 1200 Infinity high-performance liquid chromatography system, equipped with a Gemini C18 column (3 μm, 110 Å, 100 × 1.0 mm, Phenomenex). Forty-eight fractions were collected and pooled into 12 for MS measurement.

LC-MS/MS method

An UltiMate 3000 RSLC nano LC system (Dionex) fitted with a trapping cartridge (μ-Precolumn C18 PepMap 100, 5 μm, 300 μm i.d.×5 mm, 100 Å) and an analytical column (nanoEase M/Z HSS T3 column 75 μm × 250 mm C18, 1.8 μm, 100 Å, Waters) was coupled directly to a Fusion Lumos (Thermo Scientific) mass spectrometer using the Nanospray Flex ion source in positive ion mode. Trapping was carried out with a constant flow of 0.05% trifluoroacetic acid at 30 μL. Subsequently, peptides were eluted via the analytical column with a constant flow of solvent A (0.1% formic acid, 3% DMSO in water) at 0.3 μL/min with increasing percentage of solvent B (0.1% formic acid, 3% DMSO in acetonitrile).

The peptides were introduced into the Fusion Lumos via a Pico-Tip Emitter 360 μm OD × 20 μm ID; 10 μm tip (CoAnn Technologies) and an applied spray voltage of 2.4 kV. The capillary temperature was set at 275 °C. Full mass scan was acquired with mass range 375 to 1500 *m/z* in profile mode in the orbitrap with resolution of 120,000. The filling time was set at maximum of 50 ms with a limitation of 4 × 105 ions. Data dependent acquisition was performed using quadrupole isolation at 0.7 *m/z*, the resolution of the Orbitrap set to 30,000 with a fill time of 94 ms and a limitation of 1 × 105 ions. A normalized collision energy of 34 was applied. Fixed first mass was set to 110 *m/z*. MS2 data were acquired in profile mode.

MS data analysis

Files were then searched using Fragpipe v20 (protein.tsv files) with MSFragger v3.8 against the Uniprot Oryza sativa japonica database (UP000059680) containing common contaminants and reversed sequences. Contaminants and reverse proteins were filtered out and only proteins that were quantified with at least 2 razor peptides (Razor.Peptides ≥ 2) were considered for the analysis. The following modifications were included into the search parameters: Carbamidomethyl (C) and TMT18 (K) as fixed modifications, Acetyl (Protein N-term), Oxidation (M) and TMT18 (N-term) as variable modifications. A mass error tolerance of 20 ppm was set for MS1 and MS2 scans. Further parameters were: trypsin as protease with an allowance of maximum 2 missed cleavages and a minimum peptide length of seven amino acids.

Log2 transformed raw TMT reporter ion intensities ("channel" columns) were first cleaned for batch effects using the

"removeBatchEffect" function of the limma package (Ritchie et al. 2015), and further normalized using the "normalizeVSN" function of the limma package. Missing values were imputed with the "knn" method using the "impute" function of the Msnbase package (Gatto and Lilley 2012). Proteins were tested for differential expression using a moderated t-test by applying the limma package ("lmFit" and "eBayes' functions). The replicate information was added as a factor in the design matrix given as an argument to the "lmFit" function of limma. Also, imputed values were given a weight of 0.01 while quantified values were given a weight of 1 in the "lmFit" function. The *t*-value output of limma for certain statistical comparisons was analyzed with the "fdrtool" function of the fdrtool packages (Strimmer 2008) to extract *P*-values and false discovery rates (*q*-values were used). A protein was annotated as a hit with a false discovery rate (fdr) smaller 0.05 and an absolute fold-change of greater 2 and as a candidate with a fdr below 0.2 and an absolute fold-change of at least 1.5.

The mass spectrometry proteomics data have been deposited to the ProteomeXchange Consortium via the PRIDE partner repository with the dataset identifier PXD056444.

Statistical analysis

Representation factor and *P*-value of overlaps between sets of DEGs was calculated at http://nemates.org/MA/progs/overlap_stats.html. The total number of genes from the Nipponbare genome was set at 37,869 (Sakai et al. 2013). Statistical tests referred to in the text were calculated with Excel or Graph Pad Prism ver.8.0.1.

Accession numbers

Sequence data from this article can be found in the GenBank/EMBL data libraries under accession numbers

Hd1 Os06g0275000/LOC_Os06g16370
Hd3a Os06g0157700/LOC_Os06g06320
RFT1 Os06g0157500/LOC_Os06g06300
Ghd7 Os07g0261200/LOC_Os07g15770
Ghd8 Os08g0174500/LOC_Os08g07740
OsPAL1 Os02g0626100/LOC_Os02g41630
OsPAL2 Os02g0626400/LOC_Os02g41650
OsPAL4 Os02g0627100/LOC_Os02g41680
OsCAD8B Os09g0400000/LOC_Os09g23540

Acknowledgments

We are grateful to the personnel of the Botanical Garden "Città Studi" for support with plant care, and to Jennifer Schwartz and Frank Stein of the EMBLEM Proteomics core facility for support with proteomic analyses.

Author contributions

F.F. designed the study and wrote the manuscript. M.B., D.C., A.B., E.B., F.D., E.F., and T.E. collected samples, performed molecular work and analyzed data. B.K., D.H., and M.C. performed the bioinformatics analysis. F.T., J.P.M., E.T., S.W., F.L.S., I.E., V.B., G.P., and C.B. interpreted the data and revised the manuscript. All authors read and approved the final manuscript.

Supplementary data

The following materials are available in the online version of this article.

Supplementary Figure S1. RNA-sequencing controls and phase enrichment of DE genes.

Supplementary Figure S2. Overlap between genes controlled by *Hd1* and the photoperiod.

Supplementary Figure S3. Gene ontology categories enriched in the *hd1* transcriptomes.

Supplementary Figure S4. Genes regulated by *Hd1* in the phenylpropanoid biosynthetic pathway.

Supplementary Figure S5. The *hd1* leaf proteome under LD and SD.

Supplementary Figure S6. Ontological categories of differentially expressed proteins.

Supplementary Table S1. List of genes differentially expressed in the *hd1-1* mutant under LD.

Supplementary Table S2. List of genes differentially expressed in the *hd1-1* mutant under SD.

Supplementary Table S3. List of proteins identified in Nipponbare wild type and *hd1-1* mutant leaves under LD and SD.

Supplementary Table S4. List of antibodies used in cell wall analysis.

Supplementary Table S5. Primers used in this study.

Funding

This work was supported by a grant of the Italian Ministry for Universities and Research (MUR, PRIN program, project n. 20153NM8RM) to F.F., by grants of the University of Milan, PSR_Linea 2_2022 and PSR_Linea 3 FLORICE_My First SEED (MUR DM 737/2021) to C.B., PSR2022 and My First Seed 325 PSRL324 DM 737/2021 MUR to G.P., and by the Agritech National Research Center and received funding from the European Union Next-GenerationEU (PIANO NAZIONALE DI RIPRESA E RESILIENZA (PNRR)—MISSIONE 4 COMPONENTE 2, INVESTIMENTO 1.4—D.D. 1032 17/06/2022, CN00000022). M.B. was supported by a post-doctoral fellowship of the University of Milan.

Conflict of interest statement. The authors declare no conflicts of interest.

Data availability

The data underlying this article are available in the article and in its online supplementary material.

References

Abelenda J, Cruz-Oró E, Franco-Zorrilla J, Prat S. Potato StCONSTANS-like1 suppresses storage organ formation by directly activating the FT-like StSP5G repressor. *Curr Biol*. 2016:26(7):872–881. https://doi.org/10.1016/j.cub.2016.01.066

Adrian J, Farrona S, Reimer JJ, Albani MC, Coupland G, Turck F. cis-regulatory elements and chromatin state coordinately control temporal and spatial expression of FLOWERING LOCUS T in Arabidopsis. *Plant Cell*. 2010:22(5):1425–1440. https://doi.org/10.1105/tpc.110.074682

An H, Roussot C, Suárez-López P, Corbesier L, Vincent C, Piñeiro M, Hepworth S, Mouradov A, Justin S, Turnbull C, *et al*. CONSTANS acts in the phloem to regulate a systemic signal that induces photoperiodic flowering of Arabidopsis. *Development*. 2004:131(15):3615–3626. https://doi.org/10.1242/dev.01231

Ballerini ES, Kramer EM. In the light of evolution: a reevaluation of conservation in the CO-FT regulon and its role in photoperiodic regulation of flowering time. *Front Plant Sci*. 2011:2:81. https://doi.org/10.3389/fpls.2011.00081

Brambilla V, Martignago D, Goretti D, Cerise M, Somssich M, de Rosa M, Galbiati F, Shrestha R, Lazzaro F, Simon R, *et al.* Antagonistic transcription factor complexes modulate the floral transition in rice. *Plant Cell*. 2017:29(11):2801–2816. https://doi.org/10.1105/tpc.17.00645

Chaves-Sanjuan A, Gnesutta N, Gobbini A, Martignago D, Bernardini A, Fornara F, Mantovani R, Nardini M. Structural determinants for NF-Y subunit organization and NF-Y/DNA association in plants. *Plant J*. 2021:105(1):49–61. https://doi.org/10.1111/tpj.15038

Cosgrove DJ. Structure and growth of plant cell walls. *Nat Rev Mol Cell Biol*. 2024:25(5):340–358. https://doi.org/10.1038/s41580-023-00691-y

Covington MF, Maloof JN, Straume M, Kay SA, Harmer SL. Global transcriptome analysis reveals circadian regulation of key pathways in plant growth and development. *Genome Biol*. 2008:9(8):R130. https://doi.org/10.1186/gb-2008-9-8-r130

Du A, Tian W, Wei M, Yan W, He H, Zhou D, Huang X, Li S, Ouyang X, D A, *et al.* The DTH8-Hd1 module mediates day-length-dependent regulation of rice flowering. *Mol Plant*. 2017:10(7):948–961. https://doi.org/10.1016/j.molp.2017.05.006

Eguen T, Ariza JG, Brambilla V, Sun B, Bhati KK, Fornara F, Wenkel S. Control of flowering in rice through synthetic microProteins. *J Integr Plant Biol*. 2020:62(6):730–736. https://doi.org/10.1111/jipb.12865

Ezquer I, Mizzotti C, Nguema-Ona E, Gotté M, Beauzamy L, Viana VE, Dubrulle N, de Oliveira AC, Caporali E, Koroney AS, *et al.* The developmental regulator SEEDSTICK controls structural and mechanical properties of the arabidopsis seed coat. *Plant Cell*. 2016:28(10):2478–2492. https://doi.org/10.1105/tpc.16.00454

Galbiati F, Chiozzotto R, Locatelli F, Spada A, Genga A, Fornara F. Hd3a, RFT1 and Ehd1 integrate photoperiodic and drought stress signals to delay the floral transition in rice. *Plant Cell Environ*. 2016:39(9):1982–1993. https://doi.org/10.1111/pce.12760

Gao H, Jin M, Zheng X-M, Chen J, Yuan D, Xin Y, Wang M, Huang D, Zhang Z, Zhou K, *et al.* Days to heading 7, a major quantitative locus determining photoperiod sensitivity and regional adaptation in rice. *Proc Natl Acad Sci U S A*. 2014:111(46):16337–16342. https://doi.org/10.1073/pnas.1418204111

Garner W, Allard H. Effect of the relative length of day and night and other factors of the environment on growth and reproduction in plants. *J Agric Res*. 1920:18:553–606. https://doi.org/10.1175/1520-0493(1920)48%3C415b:EOTRLO%3E2.0.CO;2

Gatto L, Lilley KS. Msnbase-an R/Bioconductor package for isobaric tagged mass spectrometry data visualization, processing and quantitation. *Bioinformatics*. 2012:28(2):288–289. https://doi.org/10.1093/bioinformatics/btr645

Gnesutta N, Kumimoto RW, Swain S, Chiara M, Siriwardana C, Horner DS, Holt BF, Mantovani R. CONSTANS imparts DNA sequence-specificity to the histone-fold NF-YB/NF-YC dimer. *Plant Cell*. 2017:29(6):1516–1532. https://doi.org/10.1105/tpc.16.00864

Gnesutta N, Mantovani R, Fornara F. Plant flowering: imposing DNA specificity on histone-fold subunits. *Trends Plant Sci*. 2018:23(4):293–301. https://doi.org/10.1016/j.tplants.2017.12.005

Gómez-Ariza J, Galbiati F, Goretti D, Brambilla V, Shrestha R, Pappolla A, Courtois B, Fornara F. Loss of floral repressor function adapts rice to higher latitudes in Europe. *J Exp Bot*. 2015:66(7):2027–2039. https://doi.org/10.1093/jxb/erv004

Goretti D, Martignago D, Landini M, Brambilla V, Gomez-Ariza J, Gnesutta N, Galbiati F, Collani S, Takagi H, Terauchi R, *et al.* Transcriptional and post-transcriptional mechanisms limit Heading Date 1 (Hd1) function to adapt rice to high latitudes. *PLoS Genet*. 2017:13(1):e1006530. https://doi.org/10.1371/journal.pgen.1006530

Hayama R, Sarid-Krebs L, Richter R, Fernández V, Jang S, Coupland G. PSEUDO RESPONSE REGULATORs stabilize CONSTANS protein to promote flowering in response to day length. *EMBO J*. 2017:36(7):904–918. https://doi.org/10.15252/embj.201693907

Hu Z, Yang Z, Zhang Y, Zhang A, Lu Q, Fang Y, Lu C. Autophagy targets Hd1 for vacuolar degradation to regulate rice flowering. *Mol Plant*. 2022:15(7):1137–1156. https://doi.org/10.1016/j.molp.2022.05.006

Hwang Y-H, Kim S-K, Lee KC, Chung YS, Lee JH, Kim J-K. Functional conservation of rice OsNF-YB/YC and Arabidopsis AtNF-YB/YC proteins in the regulation of flowering time. *Plant Cell Rep*. 2016:35(4):857–865. https://doi.org/10.1007/s00299-015-1927-1

Itoh H, Nonoue Y, Yano M, Izawa T. A pair of floral regulators sets critical day length for Hd3a florigen expression in rice. *Nat Genet*. 2010:42(7):635–638. https://doi.org/10.1038/ng.606

Ivakov A, Flis A, Apelt F, Fünfgeld M, Scherer U, Stitt M, Kragler F, Vissenberg K, Persson S, Suslov D. Cellulose synthesis and cell expansion are regulated by different mechanisms in growing arabidopsis hypocotyls. *Plant Cell*. 2017:29(6):1305–1315. https://doi.org/10.1105/tpc.16.00782

Jefferson RA, Kavanagh TA, Bevan MW. GUS fusions: beta-glucuronidase as a sensitive and versatile gene fusion marker in higher plants. *EMBO J*. 1987:6(13):3901–3907. https://doi.org/10.1002/j.1460-2075.1987.tb02730.x

Jing CY, Zhang FM, Wang XH, Wang MX, Zhou L, Cai Z, Han JD, Geng MF, Yu WH, Jiao ZH, *et al.* Multiple domestications of Asian rice. *Nat Plants*. 2023:9(8):1221–1235. https://doi.org/10.1038/s41477-023-01476-z

Kawahara Y, de la Bastide M, Hamilton JP, Kanamori H, Mccombie WR, Ouyang S, Schwartz DC, Tanaka T, Wu J, Zhou S, *et al.* Improvement of the oryza sativa nipponbare reference genome using next generation sequence and optical map data. *Rice*. 2013:6(1):4. https://doi.org/10.1186/1939-8433-6-4

Kim SJ, Chandrasekar B, Rea AC, Danhof L, Zemelis-Durfee S, Thrower N, Shepard ZS, Pauly M, Brandizzi F, Keegstra K. The synthesis of xyloglucan, an abundant plant cell wall polysaccharide, requires CSLC function. *Proc Natl Acad Sci U S A*. 2020:117(33):20316–20324. https://doi.org/10.1073/pnas.2007245117

Kim S-K, Park H-Y, Jang YH, Lee KC, Chung YS, Lee JH, Kim J-K, K SK, P HY, J YH, *et al.* OsNF-YC2 and OsNF-YC4 proteins inhibit flowering under long-day conditions in rice. *Planta*. 2016:243(3):563–576. https://doi.org/10.1007/s00425-015-2426-x

Komiya R, Ikegami A, Tamaki S, Yokoi S, Shimamoto K. Hd3a and RFT1 are essential for flowering in rice. *Development*. 2008:135(4):767–774. https://doi.org/10.1242/dev.008631

Komiya R, Yokoi S, Shimamoto K. A gene network for long-day flowering activates RFT1 encoding a mobile flowering signal in rice. *Development*. 2009:136(20):3443–3450. https://doi.org/10.1242/dev.040170

Koo B-H, Yoo S-C, Park J-W, Kwon C-T, Lee B-D, An G, Zhang Z, Li J, Li Z, Paek N-C. Natural variation in OsPRR37 regulates heading date and contributes to rice cultivation at a wide range of latitudes. *Mol Plant*. 2013:6(6):1877–1888. https://doi.org/10.1093/mp/sst088

Lee R, Baldwin S, Kenel F, McCallum J, Macknight R. FLOWERING LOCUS T genes control onion bulb formation and flowering. *Nat Commun*. 2013:4(1):2884. https://doi.org/10.1038/ncomms3884

Leutert M, Rodríguez-Mias RA, Fukuda NK, Villén J. R2-P2 rapid-robotic phosphoproteomics enables multidimensional cell signaling studies. *Mol Syst Biol*. 2019:15(12):e9021. https://doi.org/10.15252/msb.20199021

Li C, Distelfeld A, Comis A, Dubcovsky J. Wheat flowering repressor VRN2 and promoter CO2 compete for interactions with NUCLEAR FACTOR-Y complexes. *Plant J*. 2011:67(5):763–773. https://doi.org/10.1111/j.1365-313X.2011.04630.x

Li Q, Yan W, Chen H, Tan C, Han Z, Yao W, Li G, Yuan M, Xing Y. Duplication of OsHAP family genes and their association with heading date in rice. *J Exp Bot*. 2016:67(6):1759–1768. https://doi.org/10.1093/jxb/erv566

Liang L, Zhang Z, Cheng N, Liu H, Song S, Hu Y, Zhou X, Zhang J, Xing Y. The transcriptional repressor OsPRR73 links circadian clock and photoperiod pathway to control heading date in rice. *Plant Cell Environ*. 2021:44(3):842–855. https://doi.org/10.1111/pce.13987

Liu C, Mao B, Yuan D, Chu C, Duan M. Salt tolerance in rice: physiological responses and molecular mechanisms. *Crop Journal*. 2022:10(1):13–25. https://doi.org/10.1016/j.cj.2021.02.010

Luccioni L, Krzymuski M, Sánchez-Lamas M, Karayekov E, Cerdán PD, Casal JJ. CONSTANS delays Arabidopsis flowering under short days. *Plant J*. 2019:97(5):923–932. https://doi.org/10.1111/tpj.14171

Lv X, Zeng X, Hu H, Chen L, Zhang F, Liu R, Liu Y, Zhou X, Wang C, Wu Z, *et al*. Structural insights into the multivalent binding of the Arabidopsis FLOWERING LOCUS T promoter by the CO-NF-Y master transcription factor complex. *Plant Cell*. 2021:33(4):1182–1195. https://doi.org/10.1093/plcell/koab016

Mockler TC, Michael TP, Priest HD, Shen R, Sullivan CM, Givan SA, Mcentee C, Kay SA, Chory J. The diurnal project: diurnal and circadian expression profiling, model-based pattern matching, and promoter analysis. *Cold Spring Harb Symp Quant Biol*. 2007:72(1):353–363. https://doi.org/10.1101/sqb.2007.72.006

Moore JP, Gao Y, Zietsman AJJ, Fangel JU, Trygg J, Willats WGT, Vivier MA. Analysis of plant cell walls using high-throughput profiling techniques with multivariate methods. *Meth Mol Biol*. 2020:2149:327–337. https://doi.org/10.1007/978-1-0716-0621-6_18

Musielak TJ, Schenkel L, Kolb M, Henschen A, Bayer M. A simple and versatile cell wall staining protocol to study plant reproduction. *Plant Reprod*. 2015:28(3–4):161–169. https://doi.org/10.1007/s00497-015-0267-1

Nakamichi N, Kusano M, Fukushima A, Kita M, Ito S, Yamashino T, Saito K, Sakakibara H, Mizuno T. Transcript profiling of an arabidopsis PSEUDO RESPONSE REGULATOR arrhythmic triple mutant reveals a role for the circadian clock in cold ctress response. *Plant Cell Physiol*. 2009:50(3):447–462. https://doi.org/10.1093/pcp/pcp004

Nemoto Y, Nonoue Y, Yano M, Izawa T. Hd1,a CONSTANS ortholog in rice, functions as an Ehd1 repressor through interaction with monocot-specific CCT-domain protein Ghd7. *Plant J*. 2016:86(3):221–233. https://doi.org/10.1111/tpj.13168

Pasriga R, Cho LH, Yoon J, An G. Identification of the regulatory region responsible for vascular tissue–specific expression in the rice Hd3a promoter. *Mol Cells*. 2018:41(4):342–350. https://doi.org/10.14348/molcells.2018.2320

Pavesi G, Mereghetti P, Mauri G, Pesole G. Weeder web: discovery of transcription factor binding sites in a set of sequences from co-regulated genes. *Nucleic Acids Res*. 2004:32(Web Server):W199–W203. https://doi.org/10.1093/nar/gkh465

Perrella G, Fasano C, Donald NA, Daddiego L, Fang W, Martignago D, Carr C, Conti L, Herzyk P, Amtmann A. Histone deacetylase Complex 1 and histone 1 epigenetically moderate stress responsiveness of Arabidopsis thaliana seedlings. *New Phytol*. 2024:241(1):166–179. https://doi.org/10.1111/nph.19165

Petroni K, Kumimoto RW, Gnesutta N, Calvenzani V, Fornari M, Tonelli C, Holt BF, Mantovani R. The promiscuous life of plant NUCLEAR FACTOR Y transcription factors. *Plant Cell*. 2012:24(12):4777–4792. https://doi.org/10.1105/tpc.112.105734

Riboni M, Galbiati M, Tonelli C, Conti L. GIGANTEA enables drought escape response via abscisic acid-dependent activation of the florigens and SUPPRESSOR OF OVEREXPRESSION OF CONSTANS. *Plant Physiol*. 2013:162(3):1706–1719. https://doi.org/10.1104/pp.113.217729

Riboni M, Test AR, Galbiati M, Tonelli C, Conti L. ABA-dependent control of GIGANTEA signalling enables drought escape via up-regulation of FLOWERING LOCUS T in Arabidopsis thaliana. *J Exp Bot*. 2016:67(22):6309–6322. https://doi.org/10.1093/jxb/erw384

Ritchie ME, Phipson B, Wu D, Hu Y, Law CW, Shi W, Smyth GK. Limma powers differential expression analyses for RNA-Sequencing and microarray studies. *Nucleic Acids Res*. 2015:43(7):e47. https://doi.org/10.1093/nar/gkv007

Sakai H, Lee SS, Tanaka T, Numa H, Kim J, Kawahara Y, Wakimoto H, Yang CC, Iwamoto M, Abe T, *et al*. Rice annotation project database (RAP-DB): an integrative and interactive database for rice genomics. *Plant Cell Physiol*. 2013:54(2):e6. https://doi.org/10.1093/pcp/pcs183

Sathitnaitham S, Suttangkakul A, Wonnapinij P, McQueen-Mason SJ, Vuttipongchaikij S. Gel-permeation chromatography–enzyme-linked immunosorbent assay method for systematic mass distribution profiling of plant cell wall matrix polysaccharides. *Plant J*. 2021:106(6):1776–1790. https://doi.org/10.1111/tpj.15255

Shapulatov U, van Zanten M, van Hoogdalem M, Meisenburg M, van Hall A, Kappers I, Fasano C, Facella P, Loh CC, Perrella G, *et al*. The mediator complex subunit MED25 interacts with HDA9 and PIF4 to regulate thermomorphogenesis. *Plant Physiol*. 2023:192(1):582–600. https://doi.org/10.1093/plphys/kiac581

Shen C, Liu H, Guan Z, Yan J, Zheng T, Yan W, Wu C, Zhang Q, Yin P, Xing Y. Structural insight into DNA recognition by CCT/NF-YB/YC complexes in plant photoperiodic flowering. *Plant Cell*. 2020:32(11):3469–3484. https://doi.org/10.1105/tpc.20.00067

Simon S, Rühl M, de Montaigu A, Wötzel S, Coupland G. Evolution of CONSTANS regulation and function after gene duplication produced a photoperiodic flowering switch in the Brassicaceae. *Mol Biol Evol*. 2015:32(9):2284–2301. https://doi.org/10.1093/molbev/msv110

Sluiter A, Hames B, Ruiz RO, Scarlata C, Sluiter J, Templeton D, Crocker D. Determination of structural carbohydrates and lignin in biomass. In: Laboratory Analytical Procedure (LAP). National Renewable Energy Laboratory; 2004.

Song YH, Shim JS, Kinmonth-Schultz HA, Imaizumi T. Photoperiodic flowering: time measurement mechanisms in leaves. *Annu Rev Plant Biol*. 2015:66(1):441–464. https://doi.org/10.1146/annurev-arplant-043014-115555

Strimmer K. Fdrtool: a versatile R package for estimating local and tail area-based false discovery rates. *Bioinformatics*. 2008:24(12):1461–1462. https://doi.org/10.1093/bioinformatics/btn209

Sun K, Huang M, Zong W, Xiao D, Lei C, Luo Y, Song Y, Li S, Hao Y, Luo W, *et al*. Hd1, Ghd7, and DTH8 synergistically determine the rice heading date and yield-related agronomic traits. *J Genet Genomics*. 2022:49:437–447. https://doi.org/10.1016/j.jgg.2022.02.018

Tamaki S, Matsuo S, Wong HL, Yokoi S, Shimamoto K. Hd3a protein is a mobile flowering signal in rice. *Science*. 2007:316(5827):1033–1036. https://doi.org/10.1126/science.1141753

Tanaka K, Murata K, Yamazaki M, Onosato K, Miyao A, Hirochika H. Three distinct rice cellulose synthase catalytic subunit genes required for cellulose synthesis in the secondary wall. *Plant Physiol*. 2003:133(1):73–83. https://doi.org/10.1104/pp.103.022442

Tiwari SB, Shen Y, Chang H, Hou Y, Harris A, Ma SF, Mcpartland M, Hymus GJ, Adam L, Marion C, *et al.* The flowering time regulator CONSTANS is recruited to the FLOWERING LOCUS T promoter via a unique cis -element. *New Phytol.* 2010:187(1):57–66. https://doi.org/10.1111/j.1469-8137.2010.03251.x

Tylewicz S, Petterle A, Marttila S, Miskolczi P, Azeez A, Singh RK, Immanen J, Mähler N, Hvidsten TR, Eklund DM, *et al.* Photoperiodic control of seasonal growth is mediated by ABA acting on cell-cell communication. *Science (1979)*. 2018:360:212–215. https://doi.org/10.1126/science.aan8576

Vicentini G, Biancucci M, Mineri L, Chirivì D, Giaume F, Miao Y, Kyozuka J, Brambilla V, Betti C, Fornara F. Environmental control of rice flowering time. *Plant Commun*. 2023:4(5):100610. https://doi.org/10.1016/j.xplc.2023.100610

Wang L, Guo K, Li Y, Tu Y, Hu H, Wang B, Cui X, Peng L. Expression profiling and integrative analysis of the CESA/CSL superfamily in rice. *BMC Plant Biol*. 2010:10(1):282. https://doi.org/10.1186/1471-2229-10-282

Wang Q, Liu W, Leung CC, Tarté DA, Gendron JM. Plants distinguish different photoperiods to independently control seasonal flowering and growth. *Science*. 2024:383:eadg9196. https://doi.org/10.1126/science.adg9196

Wang W, Mauleon R, Hu Z, Chebotarov D, Tai S, Wu Z, Li M, Zheng T, Fuentes RR, Zhang F, *et al.* Genomic variation in 3,010 diverse accessions of Asian cultivated rice. *Nature*. 2018:557(7703):43–49. https://doi.org/10.1038/s41586-018-0063-9

Wei H, Wang X, He Y, Xu H, Wang L. Clock component OsPRR73 positively regulates rice salt tolerance by modulating OsHKT2;1 -mediated sodium homeostasis. *EMBO J*. 2021:40(3):e105086. https://doi.org/10.15252/embj.2020105086

Wei H, Xu H, Su C, Wang X, Wang L. Rice CIRCADIAN CLOCK ASSOCIATED 1 transcriptionally regulates ABA signaling to confer multiple abiotic stress tolerance. *Plant Physiol*. 2022:190:1057–1073. https://doi.org/10.1093/plphys/kiac196

Wei X, Xu J, Guo H, Jiang L, Chen S, Yu C, Zhou Z, Hu P, Zhai H, Wan J. DTH8 suppresses flowering in rice, influencing plant height and yield potential simultaneously. *Plant Physiol*. 2010:153(4):1747–1758. https://doi.org/10.1104/pp.110.156943

Wenkel S, Turck F, Singer K, Gissot L, Le Gourrierec J, Samach A, Coupland G. CONSTANS and the CCAAT box binding complex share a functionally important domain and interact to regulate flowering of Arabidopsis. *Plant Cell*. 2006:18(11):2971–2984. https://doi.org/10.1105/tpc.106.043299

Xue W, Xing Y, Weng X, Zhao Y, Tang W, Wang L, Zhou H, Yu S, Xu C, Li X, *et al.* Natural variation in Ghd7 is an important regulator of heading date and yield potential in rice. *Nat Genet*. 2008:40(6):761–767. https://doi.org/10.1038/ng.143

Yang Y, Fu D, Zhu C, He Y, Zhang H, Liu T, Li X, Wu C. The RING-finger ubiquitin ligase HAF1 mediates heading date 1 degradation during photoperiodic flowering in rice. *Plant Cell*. 2015:27(9):2455–2468. https://doi.org/10.1105/tpc.15.00320

Yano M, Katayose Y, Ashikari M, Yamanouchi U, Monna L, Fuse T, Baba T, Yamamoto K, Umehara Y, Nagamura Y, *et al.* Hd1, a major photoperiod sensitivity quantitative trait locus in rice, is closely related to the Arabidopsis flowering time gene CONSTANS. *Plant Cell*. 2000:12(12):2473–2484. https://doi.org/10.1105/tpc.12.12.2473

Yuan N, Balasubramanian VK, Chopra R, Mendu V. The photoperiodic flowering time regulator fkf1 negatively regulates cellulose biosynthesis. *Plant Physiol*. 2019:180(4):2240–2253. https://doi.org/10.1104/pp.19.00013

Zambelli F, Pesole G, Pavesi G. Pscan: finding over-represented transcription factor binding site motifs in sequences from co-regulated or co-expressed genes. *Nucleic Acids Res*. 2009:37(suppl_2):W247–W52. https://doi.org/10.1093/nar/gkp464

Zheng T, Sun J, Zhou S, Chen S, Lu J, Cui S, Tian Y, Zhang H, Cai M, Zhu S, *et al.* Post-transcriptional regulation of Ghd7 protein stability by phytochrome and OsGI in photoperiodic control of flowering in rice. *New Phytol*. 2019:224(1):306–320. https://doi.org/10.1111/nph.16010

Zong W, Ren D, Huang M, Sun K, Feng J, Zhao J, Xiao D, Xie W, Liu S, Zhang H, *et al.* Strong photoperiod sensitivity is controlled by cooperation and competition among Hd1, Ghd7 and DTH8 in rice heading. *New Phytol*. 2021:229(3):1635–1649. https://doi.org/10.1111/nph.16946